筑波大学

University of Tsukuba

博士（人間生物学）学位論文

Ph.D. dissertation in Human Biology

MafB is essential in macrophages for regulating Brown Adipose Tissue's cold-induced Neuronal arborizations.

(マクロファージにおける MafB は褐色脂肪組織への交感神経発達を促し体温調節を制御する)

2019

筑波大学グローバル教育院

School of Integrative and Global Majors in the University of Tsukuba

PhD. Program in Human Biology

Manoj Kumar Yadav

Table of Contents

MafB is essential in macrophages for regulating Brown Adipose Tissue's cold-induced Neuronal arborizations.

Abstract

Obesity becomes an epidemic disease in modern times. The population of the overweight raised up to 39 % as per the World Health Organization (WHO) 2016 report. Interestingly, the WHO data indicates the countries are having a higher prevalence of obesity mostly have a cold climatic environment. To solve the high prevalence of obesity in cold climatic regions, there is a need for more exploration cause behind and finding out new possible drug targets to burn extra calories consumed.

Here in our current study, we have identified a new pathway that can be beneficial for our understanding of increasing thermogenic metabolism for a healthier life. In our current study, we have found *Mafb* in macrophages suppresses proinflammatory cytokine *Il6* and could increase sympathetic neurons in Brown Adipose Tissue (BAT). We used macrophage-specific *Mafb* deficient mice, which show a deficiency in cold adaptation and thermogenic metabolism, with increased *Il6* expression. The increased Il6 expression further suppresses an important neurotrophin hormone of BAT and end up with compromised neuronal plasticity upon cold induction, which finally reduces the BAT functions. While, when we treated this mouse with IL6-Receptor blocker, the mouse can restore his compromised ability for cold adaptation.

General Introduction

1. Types of Adipose Tissues:

Adipose tissue, also called fat tissue, comprises a large chunk of average adult body composition, and the percentage of adipose tissue mass varies between age, gender, sex, and health conditions [1–3]. Adipose tissue was primarily thought to be an inert fat-storing connective tissue up to the mid of the 20th century[4]. Later understandings of Adipose tissues categorized it as an essential organ for survival and physiological functions in the body. Moreover, the Adipose tissues classified into as many subtypes over the period. The Adipose tissues are primarily categorized into Brown Adipose Tissue (BAT) and White Adipose Tissue (WAT), based on the fat content and morphology of both subtypes [5].

a) White Adipose Tissue:

White Adipose Tissue (WAT) covers the majority of the adipose tissue mass, and it plays throughout the various compartments of the body. WAT contains up to 95% of fat content in unilocular lipid vacuoles, and the primary function of WAT is to store fat when it gets excess due to positive energy balance and release the stored fat while negative energy balance in the body[6]. The WAT is distinguished as visceral or subcutaneous. The visceral WAT is metabolically more active than the subcutaneous WAT, whereas there is a prevalence of higher fat accumulation in diseased conditions like insulin resistance or metabolic disbalance. The depots for both visceral and subcutaneous WAT might differ between mice and Humans. Likewise, in mouse, the biggest depot for visceral WAT is epididymal/gonadal WAT, while in Human gonadal WAT is not so abundant, instead, omental WAT is more profound. Similarly, for the subcutaneous WAT the more

profound depot is inguinal WAT, while in humans, the most abundant is abdominal and gluteal WAT[7].

b) Brown Adipose Tissue:

Brown Adipose Tissue (BAT) is less abundant and constitute a tiny fraction of mass in rodents about 2.5 % of their body weight, while in adult human it is a much smaller amount. However, the energy expenditure for thermogenesis by BAT while active state during cold exposure is significant in both rodents and humans. Moreover, BAT adipocytes are multilocular and store less fat with comparison to WAT, and the primary function of BAT is to do thermogenesis by uncoupled oxidative phosphorylation using a special protein "Ucp1" (Mitochondrial Uncoupling Protein 1) for sustaining cold environment [8,9]. The thermogenic program of BAT is triggered by a cold-sensation signal from the skin to hypothalamic preoptic area-specific neurons, which upon sensing cold exposure increase the sympathetic firing of catecholamine in BAT. BAT tissue expresses β3 receptors for catecholamine binding, which induces thermogenic signal cascade and induction of various thermogenic response elements in BAT, including *Ucp1*[10].

The BAT was a much-ignored topic of interest and was thought to be only crucial for hibernating animals until 1965s when the role of BAT was first indicated in human newborn infants for non-shivering thermogenesis [11]. Furthermore, the significance of BAT has gained its potentials as a possible target organ for curbing metabolic diseases in adult human in 2009, when many of the publication has demonstrated the importance of BAT in adult human health [12–14].

The primary location of BAT depot in rodents and human infants are interscapular, subscapular, axillary and cervical regions, among them interscapular BAT (iBAT) is a major depot

and most metabolically active for rodents as well as human infants, might not be an as active state in an adult human. In the adult human, major active-BAT depots reported are cervical, supraclavicular, and paravertebral depots [12,15,16].

c) Beige / Brite Adipose Tissue:

Beige / Brite Adipose tissues (bgAT) are brown-like adipose tissue appeared within many of the WAT depots after cold exposed condition, especially in the subcutaneous depots of WAT with a much higher level of Ucp1 content as a comparison to typical WAT. The bgAT was reported in earlier studies as convertible WAT with brown like features. Conversely, in recent studies, the term bgAT has gained popularity because of the identification of distinguishable parameters to differentiate WAT and bgAT, with reports that adult humans might have bgAT instead of classical BAT [17–19]. However, some more recent advancement has indicated the presence of both classical BAT and bgAT in the adult human, while human infants have proper classical BAT in the interscapular region similar to small mammals [20,21].

2. Origin of Adipose tissues

The current understanding of the origin of BAT, WAT, and bgWAT illustrates the distinct source of all the subtypes of Adipose tissues. BAT's adipocytes originate from Myf5 (Myogenic factor 5) positive myogenic precursors, where the *Prdm16* (PRD1-BF-1-RIZ1 homologous containing protein-16) expression shifts the myogenic precursor's differentiation towards brown adipocytes [22]. In contrast, the WAT and bgWAT are derived from Myf5 negative distinctive subpopulations of MSCs cells (Mesenchymal pluripotent stem cells), provided that Tmem26 high or Cd137 positive adipocytes can transdifferentiate into brown-like multilocular beige adipocytes

by cold induction, while Tmem26 low or Cd137 negative carries the unilocular WAT features [17,23].

3. Transcriptional regulation of Adipose tissues

a) Pan-Adipocyte transcriptional regulation

Pparγ (Peroxisome proliferator-activated receptor-γ) and C/Ebp's (CCAAT/enhancer-binding proteins) transcriptional regulators are critical for adipogenesis of all subtypes of adipose tissue despite their distinct physiological functions and origin. C/Ebpβ and C/Ebpδ isotypes of C/Ebp's transcription factors are expressed during the early phase of adipogenesis and indispensable for adipocytes differentiation during adipogenesis. C/Ebpβ and C/Ebpδ expression initiate the expression of C/Ebpα and Pparγ, which plays an essential role in maturation, functional maintenance, and survival of adipocytes. Interestingly, most of the adipogenesis genes have both the binding sites of C/Ebpα and Pparγ, which suggests their closer association and importance in adipose regulation [24–28].

Moreover, during preadipocyte commitment and early transcriptional cascade which induces the two key (C/Ebpα and Pparγ) transcriptional regulator includes; Ap-1 (Activated protein -1) family members, Stat5 of Stat (Signal transducer and activators of transcription) family, Egr2/Krox20 (Early growth response protein2), GR (Glucocorticoid receptor), Ebf1 of Ebf (Early B-cell factors) family member, Klf4 and Klf5 of Klf (Kruppel-like factors) family member, and NfIA & NfIB of NfI (Nuclear factor I) [27,29].

Consequently, after induction and commitment of preadipocytes, which induces C/Ebpα and Pparγ expression and initiates several other transcriptional regulators, which further increases

the Pparγ activity or independently play many important roles in the lipogenesis and adipogenesis transcriptional cascade or regulates metabolic maintenance factors during adipocytes maturation and functions. Likewise, Srebp-1 and Srebp-2 of Srebp/Adp family (Sterol regulatory element-binding protein / Adipocyte determination and differentiation dependent factor 1) act to increase the adipogenic and lipogenic activity of Pparγ by regulating transcription activity Fas (Fatty acid synthase) and Lpl (lipoprotein lipase) [30,31]. Similarly, Stat5 is expressed with C/Ebpα and Pparγ, important for Gh (growth hormone) and cytokine sensing transcriptional activation of effector adipogenic genes. Knockout of Stat5 in adipocyte impair the adipose functional by decreasing the insulin sensitivity and lipolysis [32–34].

b) Brown, Beige specific transcriptional regulation

The major transformation from typical adipose program towards brown/beige like is regulated by Prdm16, Egf2, Tgfβ superfamily BMP7 (Bone morphogenetic protein 7), Pgc1α (Pparγ transcriptional coactivator 1 α) and FoxC2 (Forkhead box C2), with cAMP-dependent Pka (Protein Kinase activity). Bmp7, FoxC2, and Egf2 expressed earlier in the preadipocyte state of BAT/bgAT, which further increase the Prdm16 expression [22,35–38]. Prdm16 is a major functional determinant of BAT by its multifunction role. Firstly, it functions as a coactivator of several brown-specific transcriptional activators, including Pgc1α, C/Ebpβ , and Pparγ by the complex formation and enrich the brown specific effector genes like Ucp1, dio2, Pgc1α, Cidea, and Elovl3 [39–41]. Secondly, it interacts with transcriptional corepressor Ehmt1 (Euchromatic histone-lysine N-methyltransferase) and silences the muscle-specific genes during brown-adipogenesis of Myf5 Positive preadipocytes [42]. Moreover, it also suppresses the white-specific

effector genes by interacting with transcriptional corepressor CtBP1 (C-terminal binding protein-1) [43].

4. Adipose Tissue Macrophages (ATM) regulation of adipose function

a) Importance of ATM

ATM has gained significant attention in the field of metabolism and adipose tissue functional & homeostasis regulation in the modern scenario. The role of ATM in metabolic disbalance and obesity was first reported in 2003, illustrating macrophages increases in adipose tissue during obesity up to 50% of adipose mass from 5% at the lean state and proinflammatory cytokines like Il-6, Tnfα & iNos induction during obesity is significantly contributed by ATM [44]. Since then, a plethora of studies have been published within this short timeframe identifying the various function of ATM; still, the enormous role and functionality of ATM in homeostasis & metabolic dysfunction are largely debatable with much more work need to be done.

b) ATM role in the homeostasis of adipose tissue function

ATM plays a crucial role in maintaining adipose tissue homeostasis by various means which includes clearance of dead adipocytes, modulate adipogenesis and lipogenesis balance, macrophages in BAT also perform unique roles in thermogenic adaptation and regulation, and macrophages provide a buffer for an excess of lipid during lipolysis and adipocyte death [45–47]. In detail, ATM digest and clear the apoptotic adipocytes for the efficient functioning of adipose tissue. However, adipocytes are way much bigger with comparison to macrophages; in that case, ATM has adopted exophagy mechanism to solve this issue by forming a crown-like structure (CLS). Where multiple macrophages encircle around the dead adipocytes to form CLS and digest

the dead adipocytes extracellularly to uptake all the content including lipid [48]. Recent studies indicated a population of macrophages attract adipose progenitor cells around the CLS by osteopontin signalling or induction activin A that facilitate the adipogenesis to maintain the turnover of adipocytes [49,50]. While the other studies indicated that the inflammatory macrophages inhibit adipogenesis in an in-vitro model, which means ATM controls the adipogenesis in either way [51]. Moreover, ATM also regulates lipogenesis by factors like AIM (Apoptosis Inhibitor of Macrophages), which can go inside the adipocyte and inhibit lipogenesis [47]. While lipolysis induced by starvation or increased metabolism triggers macrophages infiltration in the adipose tissue to uptake the excess of free fatty acids (FFA) [52]. Overall, with this recent advancement in field ATM study shows macrophages are the key regulator of adipose functions.

c) ATM specialized role in cold-induced thermogenesis

In addition to the core functionality of macrophages regulating metabolism, the recent developments include some specialized role of ATM facilitating BAT thermogenesis. Firstly, ATM guides tissue innervation of sympathetic neurons by macrophages PlexinA4 and sympathetic neuronal Sema6A interaction [53]. Secondly, the sympathetic nerve associated macrophages of BAT expresses Slc6A2 (Solute carrier family 6 members 2) to import norepinephrine and further metabolise the catecholamine by expressing MaoA (Mono-amino oxidase enzyme A)[54].

d) M1 and M2 paradigm of Macrophages and obesity

M2 or alternatively activated macrophages expressing anti-inflammatory genes like Il-10, Mrc2, Ym1, Mgl1/2 and can be distinguished using CD11b-positive, F4/80-Positive pan macrophage marker with CD206 or CD301 positive population. The M2 type macrophages are

predominately higher in a lean or healthy state both in mouse and human [45]. While during abnormal or obese conditions due to excess of lipid, adipocytes become enlarged and expand abnormally. However, the blood vessels do not increase synchronically, and this led to a decrease in oxygen and nutrient supplies to adipocytes. The adiponectin cytokine from adipocytes, which supports M2 like activation of macrophages, declines in this condition. The dying and stressed adipocytes in this situation promotes M1-like proinflammatory macrophages activation. M1 type macrophages can be distinguished using CD11C -positive, iNos Positive, or MhcII high population by cell cytometry concurrent with regular macrophage marker [45,55,56]. M1 type Macrophages express pro-inflammatory cytokines like Il6, Ilβ, Mcp1, and others. Which further recruits more monocytes in the macrophages and with reduction of insulin sensitivity [46].

e) Role of MafB in Macrophages.

MafB, also called v-maf musculoaponeurotic fibrosarcoma oncogene homolog B, belongs to the maf oncogene family is a bZip transcription factor that can recognize MARE (Maf-recognition element) sequence to bind in DNA at the promoter region of regulating genes [57]. MafB is expression is induced in the myeloid lineage of hematopoietic stem cells during differentiation from multipotent progenitors of macrophages [58]. Recent studies have shown that; MafB is essential for various functions of macrophages, including clearance of apoptotic cells by regulating C1q genes and induction of AIM protein expression increases atherosclerotic development [59,60]. Conversely in adipose tissue expression of AIM is beneficial and inhibits lipogenesis, and accordingly, the mice deficient in *Mafb* in macrophages develop obesity upon high-fat diet feeding [47,61].

5. Overview and objective of the study

Obesity becomes an epidemic disease in modern times. The population of the overweight raised up to 39 % as per the World Health Organization (WHO) 2016 report. Interestingly, the WHO data indicates the countries are having a higher prevalence of obesity mostly have a cold climatic environment. To solve the high prevalence of obesity in cold climatic regions, there is a need for more exploration cause behind and finding out new possible drug targets to burn extra calories consumed.

BAT has gained the focus of studies during the last decade as this organ is highly metabolically active and burns a significantly high amount of calories to maintain the optimum body temperature in rodents [62]. Multiple reports have been published during the last decade identifying the distribution and presence of metabolically active brown adipose tissue in the adult human. Moreover, the reports indicate the presence of active BAT is highly correlated to BMI, age, and outdoor temperature [9,63]. Cold exposure activates the outflow of sympathetic outflow as well as neuronal arborization in the adipose tissue for maintaining active state [64]. BAT is highly innervated with sympathetic neurons which secretes catecholamine to upregulate the thermogenesis when exposed to cold. It has been reported earlier that reduced neuronal innervation in BAT can develop into an inactive state and contribute to obesity. The recent reports show innervation of neurons could be regulated by macrophages [53]. However, the role of the macrophage in the neuronal remodeling of BAT needs to be more investigated to unveil the depth of molecular mechanism behind.

Here, we report MafB in macrophages is one of the regulators of cold-induced increased neuronal innervation in BAT. The macrophage-specific *Mafb* deficient mouse shows decrease thermogenesis and energy expenditure with reduced neuronal innervation in BAT. Our model

shows *Mafb* is induced after cold exposure and suppresses the pro-inflammatory cytokine Il6 expression, and the Il6 might negatively regulate the cold-induced increased neuronal branching in BAT. We could able to rescue experiment using Il6r antibody in macrophage-specific Mafb deficient mice for cold-induced thermogenesis and energy expenditure.

Materials and Methods

1. Animals

The macrophage-specific *Mafb* deficient mice (*MϕMafb*$^{-/-}$) used in this study were obtained by mating *Mafb*$^{f/f}$ and Lysm^{Cre} - Knocking to get *Mafb*$^{f/f}$-Lysm^{Cre} mice. The *Mafb*$^{f/f}$ and Lysm^{Cre} - Knocking mice were already created in our laboratory and described in previous studies [61,65]. The Genotypes were detected by a PCR-based assay using the tail tissue DNA. The genotyping primer sequences used are Cre8: 5'-CCCAGAAATGCCAGATTACG-3', NLSCre: 5'-CCCAAGAAGAAGAGGGTGTCC-3', LysM-forward 5'CCATTATTTCACAGCAGCATTGC-3', LysM-rev 5'-GCTGACTCCATAGTAGCCAG-3'. The wild type mice used in this study were purchased from SLC of C57BL/6J. All the mice were maintained under specific pathogen-free conditions in a laboratory animal resource center at the University of Tsukuba. All experiments were performed in compliance with relevant Japanese and institutional laws and guidelines and were approved by the University of Tsukuba animal ethics committee.

2. Cold exposure experiments

The protocol for the cold exposure experiments to the mice used in this study was pre-approved by the University of Tsukuba animal ethics committee, and the mice were gradually shifted to 4°C by decreasing temperature. The acute cold exposure study for 4 hours 8°C was done after intermittent cold exposure on alternate days at 8°C for up to 8 hours on the day, and after habituation of the mice, mice were challenged for acute cold exposure. The 24-hour cold exposure experiments were done under slowly decreasing temperature up to 4°C over the period of 24-hour. The ten days continuous cold exposure experiments at 4°C were done after three days gradually decreasing temperature and set up to 4°C

3. The measurement of rectal temperature

The rectal temperature of mice was measured by using a thermistor (SK-1260, skSATO). The probe was lubricated with mineral oil before inserting it into the rectum of the mice to a depth of 2 Cm.

4. VO2 / VCO2 measurement.

To measure the VO2 / VCO2, the mice ten days cold exposed were shifted to the Shoda-Laboratory within the Laboratory of the Animal Centre, and the VO2 /VCO2 were measured under the cold condition and after the injection of the CL316,243 β3 agonist drug (abcam ab144605). So, we can record and compare the optimum BAT functioning between *Mafb*$^{f/f}$ and Mϕ*Mafb*$^{-/-}$ mice.

5. RT-PCR (Real-Time – PCR).

The interscapular BAT in mice was taken and put into the liquid nitrogen immediately and transferred to -80°C for storage. Before, the analysis of the sample was crushed using a mortar and pestle frizzed in liquid nitrogen. Total RNA was extracted using ISOGEN (Nippon Gene, Tokyo, Japan). cDNA was synthesized using the QuantiTect Reverse Transcription Kit (Qiagen). The mRNA level of *Nephrin* and *Podocin* was examined by RT-qPCR using the Thermal Cycler Dice Real-Time System (Takara Bio) with THUNDERBIRD SYBR qPCR Mix (TOYOBO). mRNA abundance was normalized to the mouse *36b4* mRNA level. Specific primer sequences are *36b4;* forward, GAGACTGAGTACACCTTCCCAC, reverse ATGCAGATGGATCAGCCAGG as a housekeeping gene. The target genes include; *Mafb;* forward, TGAATTTGCTGGCACTGCTG, reverse AAGCACCATGCGGTTCATACA, *Ucp1* forward AGGGCCCCCTTCATGAGGTC, reverse GTGAAGGTCAGAATGCAAGC, *Arg1* forward TGGCTTGCGAGACGTAGAC, reverse GCTCAGGTGAATCGGCCTTTT, *Ngf* forward GAGACTCCACTCACCCCGTG, reverse TGCTCCGGTGAGTCCTGTTG, *Leptin;* forward GAGACCCCTGTGTCGGTTC,

reverse ATGAAGTCCAAGCCAGTGACC, *Adbrβ3;* forward AACCAGAAGCCCTCAGCATC, reverse CTCCTTCCTGGCAGAACCTG, *Pparγ*; forward CCTTCTAACTCCTCATGGC, reverse CATTGTGAGACATCCCCACA, *Prdm16*; forward CAGCACGGTGAAGCCATTC, reverse GCGTGCATCCGCTTGTG, *Cidea*; forward ATCACAACTGGCCTGGTTACG, reverse TACTACCCGGTGTCCATTTCT, *Vegfr2;* forward CAGTGGGATGGTCCTTGCAT, reverse ACGGTGGTGTCTGTGTCATC, *Pgc1a*; forward CCTGCCATTGTTAAGACC, reverse TGCTGCTGTTCCTGTTTTC, *Cox7a1;* forward AGAAAACCGTGTGGCAGAGA, reverse CAGCGTCATGGTCAGTCTGT, *Mac1;* forward ATGGACGCTGATGGCAATACC, reverse TCCCCATTCACGTCTCCCA, *F4/80*; forward CCCAGCTTCTGCCACCTGCA, reverse GCAGCCATTCAAGACAAAGCC, *Il1β;* forward CAACCAACAAGTGATATTCTCCATG, reverse GATCCACACTCTCCAGCTGCA, *Il6* forward CACAGAGGATACCACTCCCAACA, reverse TCCACGATTTCCCAGAGAACA.

6. RNA-Sequencing.

RNA sequencing samples were processed similarly as RT-PCR samples, after that, the sample was transferred to the RNA-Sequencing facility at Tsukuba University. The raw data were analyzed using EdgeR to determine differentially upregulated or downregulated genes p-value used were less than 0.05, and q value was less than 0.2.

7. Gene ontology.

To do the functional analysis of RNA-Sequencing differentially upregulated or downregulated genes. We used Enrichr online tools, which is a free open source tool for gene set analysis. Enrichr contains 180184 annotated gene sets from 102 gene set analyses, including WikiPathway, KEGG, GO Molecular Function, and Mouse gene atlas, which we used in our study [66,67].

8. Immunohistochemistry (IHC)

Brown adipose tissue was fixed in 10% formalin neutral buffer (Mildform, Fujifilm) overnight at 4°C, and moved it into 100% methanol to dehydrate for 8-10 hours. Then the tissue was processed accordingly to already a well-established protocol for paraffin embedding. After embedding and making block tissue were sliced using microtome and 5mm thin section slides were made for the IHC analysis. The slides were kept under 37°C overnight for proper attachment of the tissue section.

Afterward, the slides were deparaffinized on the day of IHC staining using xylene and ethanol. The antigen was retrieved using TE buffer ph 9.0 by autoclaving 2-10 min at 121°C. Antigen recovered tissue slides were blocked with secondary antibody host species 10% serum, including 1% BSA, 3% skim milk as a stabilizer and efficient blocking. 0.02% sodium azide was added as a preservative, and 0.1% Triton is used for enhancing the penetration of the antibody. The primary antibody incubation was usually 2-3 hours at room temperature or 4°C overnight, followed by washing and secondary antibody incubation at room temperature for one hour. After washing, the tissues were mounted with fluoromount media. Nuclear staining was achieved using Hoechst (2ug/ml, 1368-F, DBS) in mounting media (fluoromount). Following primary and secondary antibodies were used in our studies; anti-Ucp1 (ab19983 abcam), Anti-Tyrosine Hydroxylase (AB152, Millipore), Anti-Mac2 (Cl8942AP, cedarlane laboratories), Alexa flour 647 Donkey anti-rat (abcam), Alexaflour 488 Donkey anti-rabbit (Invitrogen), Alexaflour 596 Donkey anti-rabbit (Invitrogen), Alexaflour 596 Chicken anti-rat (Invitrogen) and Alexaflour 488 Goat anti-rabbit (Invitrogen). All the images were taken using a Keyence BZ-X 810 fluorescence microscope and analyzed by BZ-X810 analyzer software for pixel and area counting of signals.

9. ELISA Il-6

Cedarlane CL89136K-96 ELISA kit was to determine IL6 concentration. The tissue lysate of BAT was made in accordance with a study published identifying approached to assess the expression of cytokine [68]. The ELISA protocol for the assay was followed in accordance with the guideline of the kit supplier, except endogenous peroxidase blocking has been done after capturing the antigen and before applying the primary antibody. The standard and sample were treated in the same manner and after the finish of ELISA. The detection was made by a plate reader at 450nm wavelength.

10. Device for the intracapsular temperature recording

Mlx90614ESF medically calibrated sensors were programmed using Adfruit GitHub online libraries to read on the Aurdino device. Furthermore, a python program was written to handle multiple devices initiating and interpreting their data to save in an excel file. The sensor was attached to mouse skin using the 3d printer printed adapter using skin glue. The system was made as that mice could freely move in the as the sensor was attached with a freely rotating pulley circuit with an ultrathin wire. The intracapsular temperature was recorded with this self-made device for up to 4 hours.

11. Hematoxylin and Eosin Staining

Brown adipose tissue was fixed in 10% formalin neutral buffer (Mildform, Fujifilm) overnight at 4°C, and moved it into 100% methanol to dehydrate for 8-10 hours. Then the tissue was processed accordingly to already a well-established protocol for paraffin embedding. After embedding and making block tissue were sliced using microtome and 5mm thin section slides were made for the IHC analysis. The slides were kept under 37°C overnight for proper attachment of the tissue section.

Afterward, the sections were deparaffinized by dipping into Xylene 100% for five minutes with three changes. The sections were hydrated by dipping into 100% ethanol two minutes with two changes, 95% ethanol two minutes one change, 70% ethanol two minutes one change, distill water five minutes one change followed by Mayer's Haematoxylin (131-09665, Wako) staining for 20 minutes. Ater the Haematoxylin staining, the section were washed in flowing tap water for one minute, followed by dipping into Differentiation solution (A3179, Sigma), stopped the differentiation solution by dipping 5 minutes into tap water, dipped for two minutes in Scott tap water (S5134, Sigma) and stopped the Scott's tap water by dipping into tap water one minute. Next, the sections were dehydrated by dipping into 70% ethanol two minutes one change, 95% ethanol one minute one change. Finally, the sections were stained with Eosin (050-06041, Wako) for two minutes. The sections were washed in 95% ethanol one minute one change, 100% ethanol five minute two change, and then the sections were cleared by dipping into 100% Xylene for five minutes three changes and mounted using D.P.X. (317616, Sigma). All the images were taken using a Keyence BZ-X 810 fluorescence microscope and analyzed by BZ-X810 analyzer software for lipid droplet size estimation.

12. Statistical Analysis

All the quantified data are presented as the mean s.e.m. The data are from one representative experiment of at least two independent experiments. Probability values were calculated by student t-test and p-value less than 0.05 considered significant.

Results

1. *Mafb* is increased in BAT after acute cold exposure to the mice

As described earlier, macrophages regulate the various function of adipose tissue, including the clearance of dead adipocytes by efferocytosis, lipid buffering, insulin sensitivity, and more. The recent studies in BAT metabolism have indicated that macrophages can control the tissue innervation of the sympathetic neuron, and also, the sympathetic associated macrophages are essential for catecholamine metabolism. At the same time, MafB has multiple roles in macrophage for their differentiation and function, so we first checked the *Mafb* and *Ucp1* expression in BAT of WT-mice of 4 hours acute cold exposure mice using RT-PCR. Interestingly, the results showed that the *Mafb* is significantly increased, followed by acute cold exposure with a concurrent increase in *Ucp1* (Fig. 1A-B). However, cold exposure also recruits many macrophages in BAT during increased thermogenesis could also be the reason for *Mafb* increased expression in the BAT as the overall proportion of the macrophages is increased. To further analyze the probable role of MafB during thermogenesis, we obtained the macrophage-specific *Mafb* deficient mice (Mϕ*Mafb*$^{-/-}$) by mating the *Mafb*$^{f/f}$ and Lysm^{Cre} - Knocking mice.

2. Mϕ*Mafb*$^{-/-}$ mice lack in thermogenic adaptability

After obtaining the Mϕ*Mafb*$^{-/-}$ mice, we had planned to do the long cold challenge and short acute cold-challenge to investigate the ability and adaptability of the Mϕ*Mafb*$^{-/-}$ mice for cold-induced thermogenesis. Mϕ*Mafb*$^{-/-}$ mice housed for ten days under cold (4ºC) have increased their body weight during the cold exposure with a similar amount of food intake with comparison to the control mice (Fig. 2A-C). Moreover, we had checked these mice rectal temperature first, and the temperature was significantly downregulated by 0.5° C (Fig. 2D), which means the Mϕ*Mafb*$^{-/-}$

mice deficient in cold-induced thermogenesis, and this deficiency could be the possible reason that Mϕ*Mafb*$^{-/-}$ mice have increased body weight even during cold acclimatization. We further confirmed the thermogenic deficiency of the Mϕ*Mafb*$^{-/-}$ mice by IR thermal camera imaging (Fig. 2E). Moreover, we did a continuous recording of intracapsular region temperature or measured the rectal temperature hourly after acute cold challenge to the mice at 8ºC using a medically calibrated IR thermal sensor (Mlx90614ESF) or using a rectal probe (Fig. 2F-H), both results showed downregulation of the body temperature of the Mϕ*Mafb*$^{-/-}$ mice. Next, we approached to test Mϕ*Mafb*$^{-/-}$ mice BAT's thermogenic activity by pharmacological activation of the BAT of the long cold-accustomized mice using β3 agonist drugs (Cl316,243) injection. We injected the β3 agonists drug 1mg/kg of mice body weight, and the mice were put on measurement for VO2 and VCO2 under cold condition. The VO2 measurement results depicted significant reduced in thermogenic energy expenditure of the Mϕ*Mafb*$^{-/-}$ mice after β3 agonist drug injection under cold (Fig. 2I, J).

3. M*ϕMafb-/-* mice BAT function is compromised.

Our results have clearly shown the thermogenic deficiency of the Mϕ*Mafb*$^{-/-}$ mice under cold conditions. While the BAT is a major organ for producing heat for maintaining the body temperature, we analyzed the iBAT of the Mϕ*Mafb*$^{-/-}$ mice on histological & functional parameters and compared them with the controlled. To asses the gross histology of iBAT of mice housed for ten days at 4ºC, we did HE staining of the iBAT and analyse the HE staining images for lipid droplet size, Mϕ*Mafb*$^{-/-}$ mice have significantly larger lipid droplet in their iBAT with comparison to the control mice (Fig 3A, 3C). This means that the Mϕ*Mafb*$^{-/-}$ mice have accumulated higher fat than the control mice. The thermogenic functional analysis of BAT's is done by IHC using anti-Ucp1 for protein content as well as RT-PCR for *Ucp1* RNA expression (Fig. 3B, D, F). The

results clearly indicated reduced Ucp1 in iBAT of the Mϕ*Mafb*$^{-/-}$ mice, which could have reduced the thermogenic capability of the Mϕ*Mafb*$^{-/-}$ mice with the reduction of *Mafb* expression in iBAT (Fig 3E).

Moreover, we further analyzed the iBAT of ten days cold exposed Mϕ*Mafb*$^{-/-}$ mice by RNA sequencing to find a mechanistic link for the downregulation of the thermogenic property of BAT. The RNA sequencing data analysis by Enrichr online tools for Gene ontology molecular pathway 2018 and Wikipathway 2016 showed that the downregulated genes were mostly related to the metabolic property of BAT and neuronal innervation (Fig. 3G-I). The other widely reported prominent marker of BAT is analysed by using RT-PCR and the result showed significant downregulation *Pparγ, Cidea* and *Vefgr2,* while *Prdm16, Pgc1a* and *Cox7a1* is downregulated mildly (Fig. 3J). In conclusion of (Fig. 3A-J), BAT functions are compromised in the Mϕ*Mafb*$^{-/-}$ mice, which could be the reason for reduced thermogenesis of Mϕ*Mafb*$^{-/-}$ mice.

4. An abnormal population of macrophages increased in MϕMafb-/- mice, expressing a high amount of proinflammatory cytokine Il-6.

The next question was arose to find out the mechanism related to *Mafb* deficiency in macrophages and reduction of the BAT functionality & thermogenesis. To asses the macrophage role in iBAT, we first did the ICH of iBAT sample of the Mϕ*Mafb*$^{-/-}$ mice and the control mice both at room temperature and housed under cold exposure for ten days. The IHC analysis of iBAT samples indicated a tendency for an increase in the number of macrophages in Mϕ*Mafb*$^{-/-}$.both in-room temperature control and under cold exposure for ten days (Fig 4A, B). In addition, the RNA sequencing of ten days cold-housed mouse and Mouse_Gene Atlas ontology analysis of upregulated genes by Enrichr tool showed an increase in macrophages specific genes (Fig. 4G, H),

while the GO_Molecular function pathway analysis showed increased in oxidative stress like genes (Fig. 4I). Further RNA analysis using RT-PCR for macrophages and inflammatory markers show a higher tendency of increase in *Mac1* expression (Fig 4C), which could be related to the number of macrophages increased, while the inflammatory markers increased slightly like *Il1β* and *Leptin* (Fig 4D). Interestingly, When we did short cold exposure and analyzed the inflammatory genes like *Il6* RNA by RT-PCR as well as protein analysis by Elisa, it showed a significantly higher amount of Il6 in 24 hour cold exposed Mϕ*Mafb*$^{-/-}$ mice's iBAT (Fig 4E, F). This suggests *Il6* upregulation during adaption for cold climate might be a critical aspect of the adaption process.

5. *MϕMafb-/-* mice could not induce *Ngf* expression after cold-induction and impaired for the cold-induced increase in neuronal density of BAT.

After finding increased *Il6* signaling in the early stages of cold-adaption in Mϕ*Mafb*$^{-/-}$ mice, we did the literature review about the implication of *Il6,* and in one in-vitro study, and found that the *Il6* inhibit the *Ngf* expression in 3T3L1 adipocytes both in mouse and human [69]. While another study has reported Ngf in BAT after the short cold challenge is upregulated, while long term cold exposure of 5 days in mice led to again reduced back to the average expression level [1]. We had found the similar results for *Il6*, as we observed an upregulation in Il6 for 24 hour cold exposed Mϕ*Mafb*$^{-/-}$ mice (Fig. 4F), while a very slight difference in *Il6* expression in ten days cold exposed Mϕ*Mafb*$^{-/-}$ mice (Fig. 4D). To analyze the hypothesis of Il6 and Ngf cross-regulation and change in neuronal plasticity of iBAT, firstly, we analyzed the neuronal density of iBAT using sympathetic neuron marker Tyrosine Hydroxylase (TH) of ten days cold exposed Mϕ*Mafb*$^{-/-}$ mice and found that the neuronal density is less abundant as a comparison to the control mice (Fig5A-B). However, at room temperature condition difference of neuronal density in BAT was not

significant, and it has increased after cold exposure. Here we hypothesized that might be *Ngf* expression during the initial stage of adaptation of cold challenge increases the neuronal density and after habituation to the cold *Ngf* expression get normalized back to the previous level. So, we checked the Ngf expression by RT-PCR and IHC at room temperature control, after 24-hour cold exposure and ten-day cold exposure. The results showed a significant increase of *Ngf* expression after 24-hour cold both at RNA and protein level, however after 10 days cold challenge, the difference is non-significant (Fig 5C-E). More interestingly, it has also been reported in previous studies that *Mafb* has a binding site and negatively regulate *Il6* in beta cells[70]. So in our hypothesis, if *Mafb* is induced in control mice after cold exposure, it suppresses *Il6* and allows the *Ngf* expression.

6. Mϕ*Mafb-/-* mice phenotype of compromised thermogenesis is rescued by IL6R antibody treatment.

Finally, we decided to rescue the thermo-compromised phenotype of Mϕ*Mafb*$^{-/-}$ mice by neutralizing *Il6* before cold exposure by blocking its receptor. We injected mouse IL6- receptor antibody as 2mg of the initial loading and 0.5 mg maintenance dose per week. The IL6receptor blocked mice showed a positive sign of recovery by maintaining their body weight after cold exposed with similar food intake (Fig 6A-B). The rectal temperature monitoring also tends to be higher in the treated mice with comparison to the PBS control Mϕ*Mafb*$^{-/-}$ mice. CL316243, a β3 agonist injection, and VO2 measurement of these mice showed that the treated mice thermogenesis is improved significantly (Fig 6D).

AT last, we have summarized the story in a pictorial summary of MafB - Il6 – Ngf-Neuronal plasticity axis of BAT.

Discussion

The neuronal plasticity of BAT might have been regulated by many factors with a positive and negative feedback mechanism and microenvironment of the BAT. Il6, as a proinflammatory cytokine induces chronic inflammation in the peripheral system and also might inhibit neuronal plasticity of BAT. While MafB and the regulator of MaB like Rxr and Rar have been implicated for positive energy balance and the studies published earlier indicate Retinoic acid could be one of the drug choices inducing vascularization and increasing beigeing of Pdfrα adipose progenitor [71]. MafB also has been reporting for regulation AIM, which promotes lipolysis and can be beneficial for fighting obesity in another way.

Moreover, MafB – Il6 axis could contribute to solving the precise mechanism of BAT neuronal plasticity. There have been many pathways proposed in the field; however, interlinking and clarity between all these pathways have to be established by continuous improvements in the area. Likewise, The macrophages Mecp2, PlnxA4 and neuronal Sem6a axis pathway regulate the neuronal innervation more on the developmental axis and not to the adaptational axis[53]. While the Clstn3b and s100b axis actively promotes the adaptive plasticity required for BAT neurons and promotes an increase in neuronal density, and this pathway is unique for the BAT's cold-induced neuronal plasticity[71]. Furthermore, another molecule Crtc3 acts for negative feedback mechanisms, similarly to Il6, and inhibits the Ngf neurotrophin of BAT, which promotes a neuronal increase in BAT [72]. Our current finding could bring better understandability for future implications of BAT neuronal axis plasticity.

AT last, even though we could be able to rescue the thermogenic deficient phenotype of *MϕMafb*$^{-/-}$ mice, we need to establish a direct link for *Il6* suppression by Mafb upregulation during

cold exposure by doing promoter binding analysis of MafB to the Il6. Moreover, we need to identify the specific population of macrophages in BAT expressing *Il6* for more clarity.

References

1. Camerino, C., Conte, E., Caloiero, R., Fonzino, A., Carratù, M., Lograno, M.D., and Tricarico, D. (2018). Evaluation of short and long term cold stress challenge of nerve grow factor, brain-derived neurotrophic factor, osteocalcin and oxytocin mRNA expression in BAT, brain, bone and reproductive tissue of male mice using real-time PCR and linear correlation analysis. Front. Physiol. *8*.

2. Jackson, A.S., Stanforth, P.R., Gagnon, J., Rankinen, T., Leon, A.S., Rao, D.C., Skinner, J.S., Bouchard, C., and Wilmore, J.H. (2002). The effect of sex, age and race on estimating percentage body fat from body mass index: The Heritage Family Study. Int. J. Obes. *26*, 789–796.

3. Gallaher, D., and S. B. Heymsfield, M. Heo, S. A. Jebb, P. R. Murgatroyd, and Y.S. (2000). Healthy percentage body fat ranges: an approach for developing guidelines based on body mass index," The American Journal of Clinical Nutrition, vol. 72, no. 3, pp. 694–701, 2000. View at Google Scholar · View at Scopus. Am. J. Clin. Nutr. *72*, 694–701.

4. Wertheimer, E., and Shapiro, B. (1948). The physiology of adipose tissue. Physiol. Rev. *28*, 451–464.

5. Hull, D., and Segall, M.M. (1966). Distinction of brown from white adipose tissue. Nature *212*, 469–472.

6. Rosen, E.D., and Spiegelman, B.M. (2014). What we talk about when we talk about fat. Cell *156*, 20–44. Available at: http://dx.doi.org/10.1016/j.cell.2013.12.012.

7. Park, A. (2014). Distinction of white, beige and brown adipocytes derived from mesenchymal stem cells. World J. Stem Cells *6*, 33.

8. Smith, R.E., and Horwitz, B.A. (1969). Brown fat biology and thermogenesis. Physiol. Rev. *49*.

9. Leitner, B.P., Huang, S., Brychta, R.J., Duckworth, C.J., Baskin, A.S., Mcgehee, S., Tal, I., Dieckmann, W., Gupta, G., Kolodny, G.M., *et al.* (2017). Mapping of human brown adipose tissue in lean and obese young men. pnas *114*, 8649–8654. Available at: www.pnas.org/cgi/doi/10.1073/pnas.1705287114 [Accessed September 25, 2019].

10. Zhang, W., and Bi, S. (2015). Hypothalamic Regulation of Brown Adipose Tissue Thermogenesis and Energy Homeostasis. Front. Endocrinol. (Lausanne). *6*.

11. Dawkins, M.J.R., and Scopes, J.W. (1965). Non-shivering thermogenesis and brown adipose tissue in the human new-born infant. Nature *206*, 201–202.

12. Cypess, A.M., Lehman, S., Williams, G., Tal, I., Goldfine, A.B., Kuo, F.C., Palmer, E.L., Tseng, Y.-H., Doria, A., Kolodny, G.M., *et al.* (2009). Identification and Importance of Brown Adipose Tissue in Adult Humans. N Engl J Med *360*, 1509–1526.

13. Virtanen, K.A., Lidell, M.E., Orava, J., Heglind, M., Westergren, R., Niemi, T., Taittonen, M., Laine, J., Savisto, N.J., Enerbäck, S., *et al.* (2009). Functional brown adipose tissue in healthy adults. N. Engl. J. Med. *360*, 1518–1525.

14. Saito, M., Okamatsu-Ogura, Y., Matsushita, M., Watanabe, K., Yoneshiro, T., Nio-Kobayashi, J., Iwanaga, T., Miyagawa, M., Kameya, T., Nakada, K., *et al.* (2009). High incidence of metabolically active brown adipose tissue in healthy adult humans: Effects of cold exposure and adiposity. Diabetes *58*, 1526–1531.

15. Schoettl, T., Fischer, I.P., and Ussar, S. (2018). Heterogeneity of adipose tissue in development and metabolic function. J. Exp. Biol. *121*.

16. Sacks, H., and Symonds, M.E. (2013). Anatomical locations of human brown adipose tissue: Functional relevance and implications in obesity and type 2 diabetes. Diabetes *62*, 1783–1790.

17. Wu, J., Boström, P., Sparks, L.M., Ye, L., Choi, J.H., Giang, A.H., Khandekar, M., Virtanen, K.A., Nuutila, P., Schaart, G., *et al.* (2012). Beige adipocytes are a distinct type of thermogenic fat cell in mouse and human. Cell *150*, 366–376.

18. Lehr, L., Canola, K., Léger, B., and Giacobino, J.P. (2009). Differentiation and characterization in primary culture of white adipose tissue brown adipocyte-like cells. Int. J. Obes. *33*, 680–686.

19. Young, P., Arch, J.R.S., and Ashwell, M. (1984). Brown adipose tissue in the parametrial fat pad of the mouse. FEBS Lett. *167*, 10–14.

20. Jespersen, N.Z., Larsen, T.J., Peijs, L., Daugaard, S., Homøe, P., Loft, A., De Jong, J., Mathur, N., Cannon, B., Nedergaard, J., *et al.* (2013). A classical brown adipose tissue mrna signature partly overlaps with brite in the supraclavicular region of adult humans. Cell Metab. *17*, 798–805.

21. Lidell, M.E., Betz, M.J., Leinhard, O.D., Heglind, M., Elander, L., Slawik, M., Mussack, T., Nilsson, D., Romu, T., Nuutila, P., *et al.* (2013). Evidence for two types of brown adipose tissue in humans. Nat. Med. *19*, 631–634.

22. Seale, P., Bjork, B., Yang, W., Kajimura, S., Chin, S., Kuang, S., Scimè, A., Devarakonda, S., Conroe, H.M., Erdjument-Bromage, H., *et al.* (2008). PRDM16 controls a brown fat/skeletal muscle switch. Nature *454*, 961–967.

23. Rosenwald, M., and Wolfrum, C. (2014). The origin and definition of brite versus white and classical brown adipocytes. Adipocyte *3*. Available at: https://www.tandfonline.com/action/journalInformation?journalCode=kadi20 [Accessed September 26, 2019].

24. Imai, T., Takakuwa, R., Marchand, S., Dentz, E., Bornert, J.-M., Messaddeq, N., Wendling, O., Mark, M., Atrice Desvergne, B., Wahli, W., *et al.* (2004). Peroxisome proliferator-activated receptor is required in mature white and brown adipocytes for their survival in the mouse Available at: www.pnas.orgcgidoi10.1073pnas.0400356101 [Accessed October 15, 2019].

25. Wu, Z., Bucher, N.L., and Farmer, S.R. (1996). Induction of peroxisome proliferator-activated receptor gamma during the conversion of 3T3 fibroblasts into adipocytes is mediated by C/EBPbeta, C/EBPdelta, and glucocorticoids. Mol. Cell. Biol. *16*, 4128–4136.

26. Tanaka, T., Yoshida, N., Kishimoto, T., and Akira, S. (1997). Defective adipocyte differentiation in mice lacking the C/EBPβ and/or C/EBPδ gene. EMBO J. *16*, 7432–7443.

27. Lee, J.-E., Schmidt, H., Lai, B., and Ge, K. (2019). Transcriptional and Epigenomic Regulation of Adipogenesis. Mol. Cell. Biol. *39*, e00601-18. Available at: https://doi.org/10.1128/MCB.00601-18. [Accessed October 11, 2019].

28. Lefterova, M.I., Zhang, Y., Steger, D.J., Schupp, M., Schug, J., Cristancho, A., Feng, D., Zhuo, D., Stoeckert, C.J., Liu, X.S., *et al.* (2008). PPARγ and C/EBP factors orchestrate adipocyte biology via adjacent binding on a genome-wide scale. Genes Dev. *22*, 2941–2952.

29. White, U.A., and Stephens, J.M. (2010). Transcriptional factors that promote formation of white adipose tissue. Mol. Cell. Endocrinol. *318*, 10–14.

30. Tontonoz, P., Kim, J.B., Graves, R.A., and Spiegelman, B.M. (1993). ADDi: a Novel Helix-Loop-Helix Transcription Factor Associated with Adipocyte Determination and Differentiation Downloaded from Available at: http://mcb.asm.org/ [Accessed October 17, 2019].

31. Kim, J.B., and Spiegelman, B.M. (1996). ADD1/SREBP1 promotes adipocyte differentiation and gene expression linked to fatty acid metabolism. Genes Dev. *10*, 1096–1107.

32. Stewart, W.C., Morrison, R.F., Young, S.L., and Stephens, J.M. (1999). Regulation of signal transducers and activators of transcription (STATs) by effectors of adipogenesis: Coordinate regulation of STATs 1, 5A, and 5B with peroxisome proliferator-activated receptor-γ and C/AAAT enhancer binding protein-α. Biochim. Biophys. Acta - Mol. Cell Res. *1452*, 188–196.

33. Shang, C.A., and Waters, M.J. (2003). Constitutively Active Signal Transducer and Activator of Transcription 5 Can Replace the Requirement for Growth Hormone in Adipogenesis of 3T3-F442A Preadipocytes. Mol. Endocrinol. *17*, 2494–2508.

34. Kaltenecker, D., Mueller, K.M., Benedikt, P., Feiler, U., Themanns, M., Schlederer, M., Kenner, L., Schweiger, M., Haemmerle, G., and Moriggl, R. (2017). Adipocyte STAT5 deficiency promotes adiposity and impairs lipid mobilisation in mice. Diabetologia *60*, 296–305.

35. Cederberg, A., Gronning, L.M., Ahrén, B., Taskén, K., Carlsson, P., and Enerbäck, S. (2001). FOXC2 is a winged helix gene that counteracts obesity, hypertriglyceridemia, and diet-induced insulin resistance. Cell *106*, 563–573.

36. Rajakumari, S., Wu, J., Ishibashi, J., Lim, H.W., Giang, A.H., Won, K.J., Reed, R.R., and Seale, P. (2013). EBF2 determines and maintains brown adipocyte identity. Cell Metab. *17*, 562–574.

37. Kajimura, S., Seale, P., and Spiegelman, B.M. (2010). Transcriptional Control of Brown Fat Development. Cell Metab.

38. Tseng, Y.H., Kokkotou, E., Schulz, T.J., Huang, T.L., Winnay, J.N., Taniguchi, C.M.,

Tran, T.T., Suzuki, R., Espinoza, D.O., Yamamoto, Y., *et al.* (2008). New role of bone morphogenetic protein 7 in brown adipogenesis and energy expenditure. Nature *454*, 1000–1004.

39. Karamitri, A., Shore, A.M., Docherty, K., Speakman, J.R., and Lomax, M.A. (2009). Combinatorial transcription factor regulation of the cyclic AMP-response element on the Pgc-1α promoter in white 3T3-L1 and brown HIB-1B preadipocytes. J. Biol. Chem. *284*, 20738–20752.

40. Kajimura, S., Seale, P., Kubota, K., Lunsford, E., Frangioni, J. V., Gygi, S.P., and Spiegelman, B.M. (2009). Initiation of myoblast to brown fat switch by a PRDM16-C/EBP-β transcriptional complex. Nature *460*, 1154–1158.

41. Shapira, S.N., and Seale, P. (2019). Transcriptional Control of Brown and Beige Fat Development and Function. Obesity *27*, 13–21.

42. Ohno, H., Shinoda, K., Ohyama, K., Sharp, L.Z., and Kajimura, S. (2013). EHMT1 controls brown adipose cell fate and thermogenesis through the PRDM16 complex. Nature *504*, 163–167.

43. Kajimura, S., Seale, P., Tomaru, T., Erdjument-Bromage, H., Cooper, M.P., Ruas, J.L., Chin, S., Tempst, P., Lazar, M.A., and Spiegelman, B.M. (2008). Regulation of the brown and white fat gene programs through a PRDM16/CtBP transcriptional complex. Genes Dev. *22*, 1397–1409.

44. Weisberg, S.P., Leibel, R.L., and Ferrante, A.W. (2003). Obesity is associated with macrophage accummulation in adipose tissue. J Clin Invest *112*, 1796–1808.

45. Catrysse, L., and van Loo, G. (2018). Adipose tissue macrophages and their polarization in health and obesity. Cell. Immunol. *330*, 114–119.

46. Boutens, L., and Stienstra, R. (2016). Adipose tissue macrophages: going off track during obesity. Diabetologia *59*, 879–894.

47. Arai, S., and Miyazaki, T. (2014). Impacts of the apoptosis inhibitor of macrophage (AIM) on obesity-associated inflammatory diseases. Semin. Immunopathol. *36*, 3–12.

48. Haka, A.S., Barbosa-Lorenzi, V.C., Lee, H.J., Falcone, D.J., Hudis, C.A., Dannenberg, A.J., and Maxfield, F.R. (2016). Exocytosis of macrophage lysosomes leads to digestion of apoptotic adipocytes and foam cell formation. J. Lipid Res. *57*, 980–992.

49. Lee, Y.H., Petkova, A.P., and Granneman, J.G. (2013). Identification of an adipogenic niche for adipose tissue remodeling and restoration. Cell Metab. *18*, 355–367.

50. Zaragosi, L.-E., Wdziekonski, B., Villageois, P., Keophiphath, M., Maumus, M., Tchkonia, T., Bourlier, V., Mohsen-Kanson, T., Ladoux, A., Elabd, C., *et al.* (2010). Activin a plays a critical role in proliferation and differentiation of human adipose progenitors. Diabetes *59*, 2513–21. Available at: http://www.ncbi.nlm.nih.gov/pubmed/20530742 [Accessed October 29, 2019].

51. Lacasa, D., Taleb, S., Keophiphath, M., Miranville, A., and Clement, K. (2007). Macrophage-secreted factors impair human adipogenesis: Involvement of

proinflammatory state in preadipocytes. Endocrinology *148*, 868–877.

52. Kosteli, A., Sugaru, E., Haemmerle, G., Martin, J.F., Lei, J., Zechner, R., and Ferrante, A.W. (2010). Weight loss and lipolysis promote a dynamic immune response in murine adipose tissue. J. Clin. Invest. *120*, 3466–3479.

53. Wolf, Y., Boura-Halfon, S., Cortese, N., Haimon, Z., Sar Shalom, H., Kuperman, Y., Kalchenko, V., Brandis, A., David, E., Segal-Hayoun, Y., *et al.* (2017). Brown-adipose-tissue macrophages control tissue innervation and homeostatic energy expenditure. Nat. Immunol. *18*, 665–674.

54. Pirzgalska, R.M., Seixas, E., Seidman, J.S., Link, V.M., Sánchez, N.M., Mahú, I., Mendes, R., Gres, V., Kubasova, N., Morris, I., *et al.* (2017). Sympathetic neuron-associated macrophages contribute to obesity by importing and metabolizing norepinephrine. Nat. Med. *23*, 1309–1318.

55. Trayhurn, P. (2013). Hypoxia and adipose tissue function and dysfunction in obesity. Physiol. Rev. *93*, 1–21.

56. CN Lumeng, J.B.A.S. (2007). Obesity induces a phenotypic switch in adipose tissue macrophage polarization. J. Clin. Invest. *117*, 175–184.

57. Kataoka, K., Fujiwara, K.T., Noda, M., and Nishizawa, M. (1994). MafB, a New Maf Family Transcription Activator That Can Associate with Maf and Fos but Not with Jun Available at: http://mcb.asm.org/ [Accessed October 30, 2019].

58. Kelly, L.M. (2000). MafB is an inducer of monocytic differentiation. EMBO J. *19*, 1987–1997.

59. Tran, M.T.N., Hamada, M., Jeon, H., Shiraishi, R., Asano, K., Hattori, M., Nakamura, M., Imamura, Y., Tsunakawa, Y., Fujii, R., *et al.* (2017). MafB is a critical regulator of complement component C1q. Nat. Commun. *8*.

60. Hamada, M., Nakamura, M., Tran, M.T.N., Moriguchi, T., Hong, C., Ohsumi, T., Dinh, T.T.H., Kusakabe, M., Hattori, M., Katsumata, T., *et al.* (2014). MafB promotes atherosclerosis by inhibiting foam-cell apoptosis. Nat. Commun. *5*, 1–14. Available at: http://dx.doi.org/10.1038/ncomms4147.

61. Tran, M.T.N., Hamada, M., Nakamura, M., Jeon, H., Kamei, R., Tsunakawa, Y., Kulathunga, K., Lin, Y.Y., Fujisawa, K., Kudo, T., *et al.* (2016). MafB deficiency accelerates the development of obesity in mice. FEBS Open Bio *6*, 540–547.

62. Nedergaard, J., Bengtsson, T., and Cannon, B. (2011). New powers of brown fat: Fighting the metabolic syndrome. Cell Metab. *13*, 238–240.

63. Ouellet, V., Routhier-Labadie, A., Bellemare, W., Lakhal-Chaieb, L., Turcotte, E., Carpentier, A.C., and Richard, D. (2011). Outdoor temperature, age, sex, body mass index, and diabetic status determine the prevalence, mass, and glucose-uptake activity of 18F-FDG-detected BAT in humans. J. Clin. Endocrinol. Metab. *96*, 192–199.

64. Jiang, H., Ding, X., Cao, Y., Wang, H., and Zeng, W. (2017). Dense Intra-adipose Sympathetic Arborizations Are Essential for Cold-Induced Beiging of Mouse White

Adipose Tissue. Cell Metab. *26*, 686-692.e3. Available at: http://www.ncbi.nlm.nih.gov/pubmed/28918935 [Accessed October 30, 2019].

65. Suzuki, T., Kelly, V.P., Motohashi, H., Nakajima, O., Takahashi, S., Nishimura, S., and Yamamoto, M. (2008). Deletion of the selenocysteine tRNA gene in macrophages and liver results in compensatory gene induction of cytoprotective enzymes by Nrf2. J. Biol. Chem. *283*, 2021–2030.

66. Chen, E.Y., Tan, C.M., Kou, Y., Duan, Q., Wang, Z., Meirelles, G. V., Clark, N.R., and Ma'ayan, A. (2013). Enrichr: Interactive and collaborative HTML5 gene list enrichment analysis tool. BMC Bioinformatics *14*.

67. Kuleshov, M. V., Jones, M.R., Rouillard, A.D., Fernandez, N.F., Duan, Q., Wang, Z., Koplev, S., Jenkins, S.L., Jagodnik, K.M., Lachmann, A., *et al.* (2016). Enrichr: a comprehensive gene set enrichment analysis web server 2016 update. Nucleic Acids Res. *44*, W90–W97.

68. Amsen, D., de Visser, K.E., and Town, T. (2009). Approaches to determine expression of inflammatory cytokines. Methods Mol. Biol. *511*, 107–142.

69. Peeraully, M.R., Jenkins, J.R., and Trayhurn, P. (2004). NGF gene expression and secretion in white adipose tissue: Regulation in 3T3-L1 adipocytes by hormones and inflammatory cytokines. Am. J. Physiol. - Endocrinol. Metab. *287*.

70. Zhu, M., Wei, Y., Geißler, C., Abschlag, K., Campos, J.C., Hristov, M., Möllmann, J., Lehrke, M., Karshovska, E., and Schober, A. (2017). Hyperlipidemia-induced MicroRNA-155-5p improves β-cell function by targeting Mafb. Diabetes *66*, 3072–3084.

71. Zeng, X., Ye, M., Resch, J.M., Jedrychowski, M.P., Hu, B., Lowell, B.B., Ginty, D.D., and Spiegelman, B.M. (2019). Innervation of thermogenic adipose tissue via a calsyntenin 3β–S100b axis. Nature *569*, 229–235.

72. Yoon, Y.-S., Tsai, W.-W., Van De Velde, S., Chen, Z., Lee, K.-F., Morgan, D.A., Rahmouni, K., Matsumura, S., Wiater, E., Song, Y., *et al.* (2018). cAMP-inducible coactivator CRTC3 attenuates brown adipose tissue thermogenesis. pnas *115*, E5289–E5297. Available at: www.pnas.org/cgi/doi/10.1073/pnas.1805257115 [Accessed October 31, 2019].

Figure legends

Figure 1. *Mafb* is increased in BAT after acute cold exposure to the mice.

Eight weeks old wild type mice accustomed to short acute exposure for one week, and on day eight, mice were exposed to 8°C for four hours, iBAT collected for RT-PCR and IHC. **A, B)** RTqPCR analysis for *Mafb* and *Ucp1* of the BAT. **C)** IHC analysis using rat-anti-mouse Mac2 monoclonal antibody and detected by using Alexaflour-647. Mice (n=4), *P<0.05, **P<0.01, ***P<0.001.

Figure 2. *MϕMafb*$^{-/-}$ mice lack in thermogenic adaptability.

Eight to ten weeks old littermate *Mafb*$^{f/f}$ and *MϕMafb*$^{-/-}$ divided into groups for each set of experiments exposed to 10 days continuous cold at 4°C or acute cold exposure for up to four at 8°C (n= 4 to 6 in each group). **A)** Bodyweight measurement of during cold exposure. **B)** Percentage of body weight change from day 1 to day 10 of cold exposure. **C)** Daily food consumption for ten days. **D)** Rectal temperature recording at day 10 of cold exposure. **E)** Thermal image using a thermal camera (Seek thermal Compact Pro). **F)** Acute cold exposure and measurement of hourly rectal temperature using the SK-1260sk SATO rectal temperature device. **G)** Continuous skin temperature recording using IR thermal sensor Mlx90614ESF-DCA-000-SP for the intracapsular region of the mice. **H)** Area under curve analysis for the continuous recorded intracapsular skin temperature of the mice**. I)** VO2 measurement of the ten days cold exposed mice under cold, after injecting β3 agonist drug CL316,243**.J)** Area under curve analysis for the selected area after the injection. *P<0.05, **P<0.01, ***P<0.001.

Figure 3. *MϕMafb*$^{-/-}$ mice BAT function is compromised.

Eight to ten weeks old littermate *Mafb*$^{f/f}$ and *MϕMafb*$^{-/-}$ divided into groups for each set of experiments exposed to 10 days continuous cold at 4°C, at day ten mice are sacrificed, and iBAT is collected for either RT-PCR, Histology analysis, IHC analysis or RNA sequencing from a different set of experiments. **A)** Hematoxylin and Eosin staining of the iBAT. **B)** IHC analysis using monoclonal Rabbit-anti mouse Ucp1 antibody, Alexflour 596 Donkey Anti-Rabbit, is used for the detection of Ucp1. **C)** Quantification of lipid droplet size of the HE staining of panel A using BZX800 software of Keyence. **D)** Quantification of Ucp1 of the IHC shown in panel B. **E, F)** RT-PCR analysis using BAT collected after ten days cold exposed mice for *Mafb* and *Ucp1* expression. **G)** Ten days cold exposed mice iBAT processed for RNA sequencing (n=3) for each group, the result has been analysed using Edge-R, the heatmap shows 108 differentially downregulated genes ($p<0.05$, $q<0.2$). **H, I)** Functional analysis using the downregulated genes by the Encrichr online tools for Gene Ontology molecular function 2018 and Wikipathway 2016. **J)** BAT specific genes analysis by using RT-PCR of the iBAT sample. *P<0.05, **P<0.01, ***P<0.001.

Figure 4. An abnormal population of macrophages increased in *MϕMafb*$^{-/-}$ mice, expressing a high amount of proinflammatory cytokine IL-6.

Eight to ten weeks old littermate *Mafb*$^{f/f}$ and *MϕMafb*$^{-/-}$ divided into groups for each set of experiments exposed to 10 days continuous cold at 4°C or room temperature control. The iBAT samples have been collected for RT-PCR, ELISA, IHC and RNA sequencing analysis from a different set of experiments. **A, B)** IHC analysis of iBAT using anti-mouse Mac2 antibody with counterstaining with anti-Rat Alexaflour647 antibody of room temperature control mice and ten days cold exposed mice respectively. **C)** RT-PCR of iBAT of ten days cold exposed mice for macrophage markers *Mac1 and F4/80,* while *Arg1* as M2 Macrophage marker. **D, E)** RT-PCR of BAT of ten days cold exposed or room temperature control mice for proinflammatory markers *Il1b, Tgfb, Leptin* and *Il-6.* **F)** Il-6 protein quantification of iBAT lysate of mice at room temperature control and the cold exposed using Mouse Il-6 Elisa Kit (Cedarlane, CL89136K-96). **G)** Ten days cold exposed mice iBAT processed for RNA sequencing (n=3) for each group, the result has been analysed using Edge-R, the heatmap shows 190 differentially upregulated genes ($p<0.05$, $q<0.2$). **H, I)** Functional analysis using the downregulated genes by the Encrichr online tools for Gene Ontology Mouse Gene Atlas and GO_Molecular Function. *P<0.05, **P<0.01, ***P<0.001.

Figure 5. *MϕMafb*$^{-/-}$ mice could not induce *Ngf* expression after cold-induction and impaired for the cold-induced increase in neuronal density of BAT.

Eight to ten-week-old littermate *Mafb*$^{f/f}$ and *MϕMafb*$^{-/-}$ mice either cold exposed at 4°C for ten days , the mice acclimatized for cold with gradual reduction of temperature up to 4°C for 24 hours, or the room temperature control has been analysed for their iBAT by RT-PCR and IHC. **A)** IHC of iBAT by using TH (Tyrosine Hydroxylase) a sympathetic neuronal marker antibody for ten days cold exposed mice. **B)** IHC of TH stained iBAT slides has been analysed for neuronal density for both room temperature controls and as well as ten days cold exposed. **C)** IHC of iBAT using NGF antibody for mouse after 24 hours of cold exposure. **D, E)** RT-PCR of iBAT for room temperature control, 24 hours cold-acclimatized and ten days cold exposed mouse.

Figure 6. *MϕMafb*$^{-/-}$ mice phenotype of compromised thermogenesis is rescued by IL6R antibody treatment.

Seven-week old *MϕMafb*$^{-/-}$ mice divided into two groups IL6R antibody injection and PBS injection and induced for continuous ten days cold exposure at 4°C. **A)** Percentage of body weight change is measured from day 1 to day 10 for both groups. B) Average daily food consumption of both groups for ten days. **C)** Rectal temperature recording on day ten. **D, E**) Oxygen consumption analysis and area under curve analysis after CL316,243 injection (a β3 agonist drug injection).

Figures

Figure 1

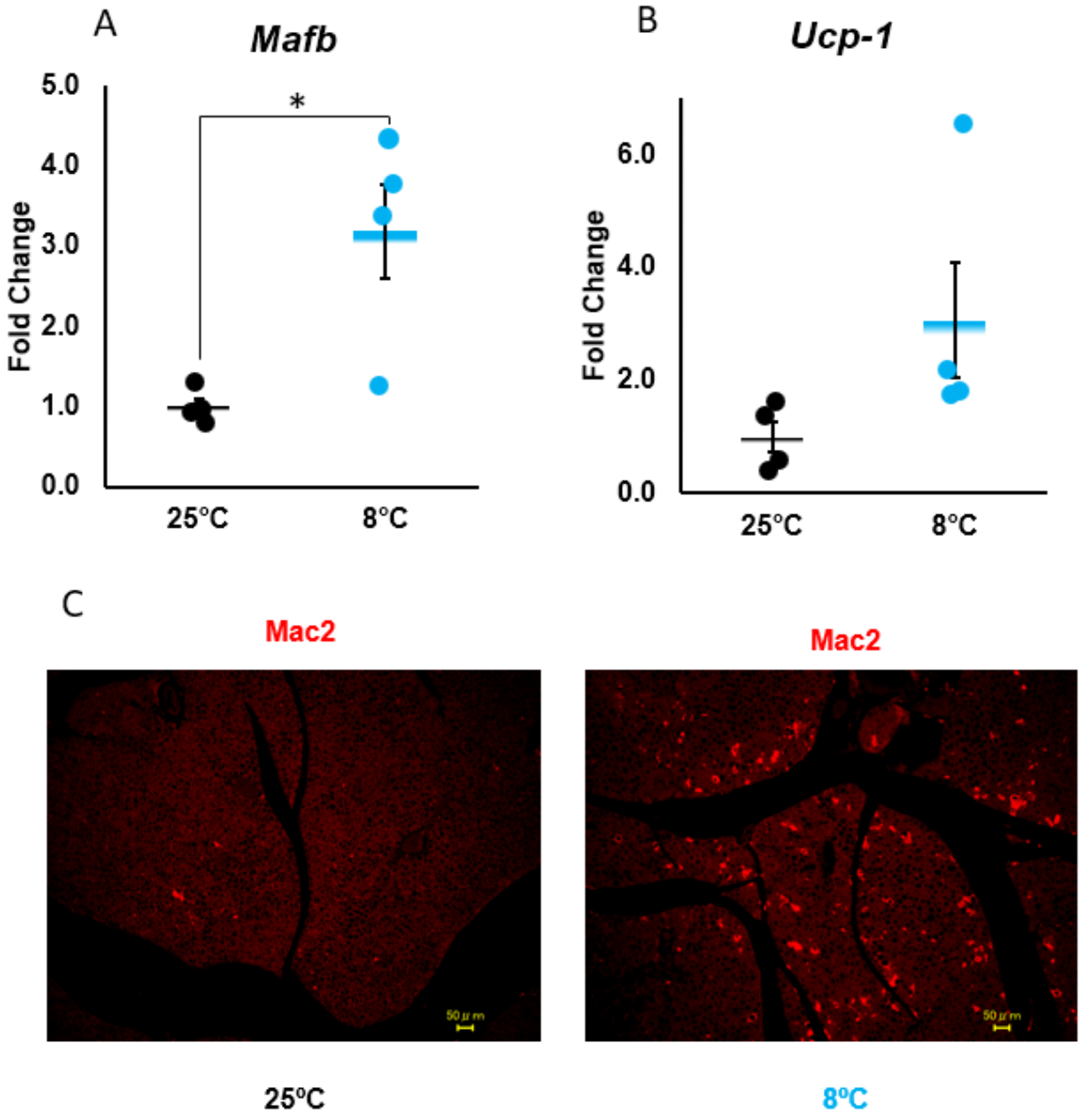

Figure 2 (A-D)

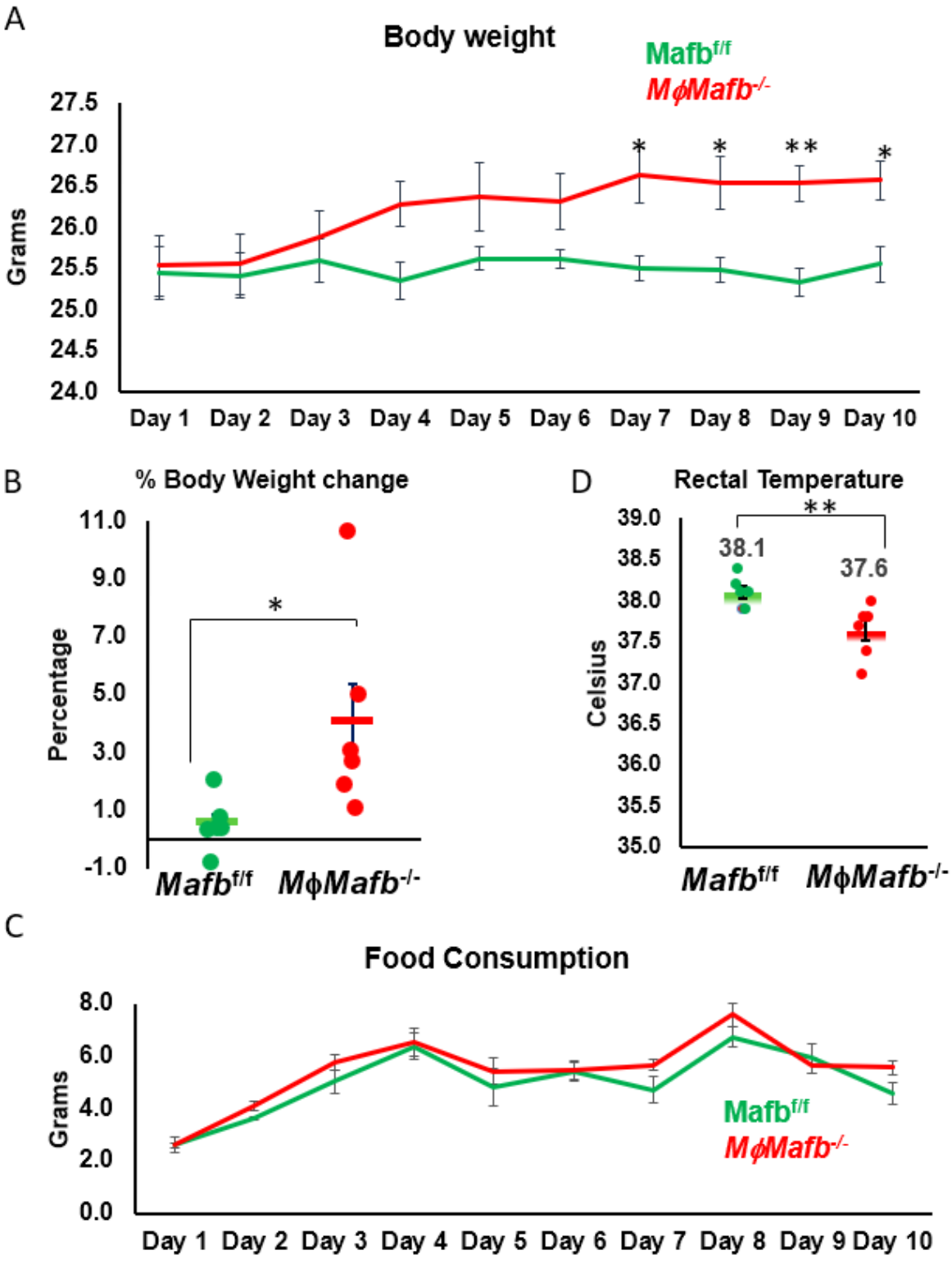
A
Body weight
Mafb f/f
MϕMafb -/-
Grams
27.5
27.0
26.5
26.0
25.5
25.0
24.5
24.0
Day 1 Day 2 Day 3 Day 4 Day 5 Day 6 Day 7 Day 8 Day 9 Day 10
B
% Body Weight change
Percentage
11.0
9.0
7.0
5.0
3.0
1.0
-1.0
Mafb f/f MϕMafb -/-
D
Rectal Temperature
Celsius
39.0
38.5
38.0
37.5
37.0
36.5
36.0
35.5
35.0
38.1
37.6
Mafb f/f MϕMafb -/-
C
Food Consumption
Grams
8.0
6.0
4.0
2.0
0.0
Mafb f/f
MϕMafb -/-
Day 1 Day 2 Day 3 Day 4 Day 5 Day 6 Day 7 Day 8 Day 9 Day 10

Figure 2 (E-G)

E

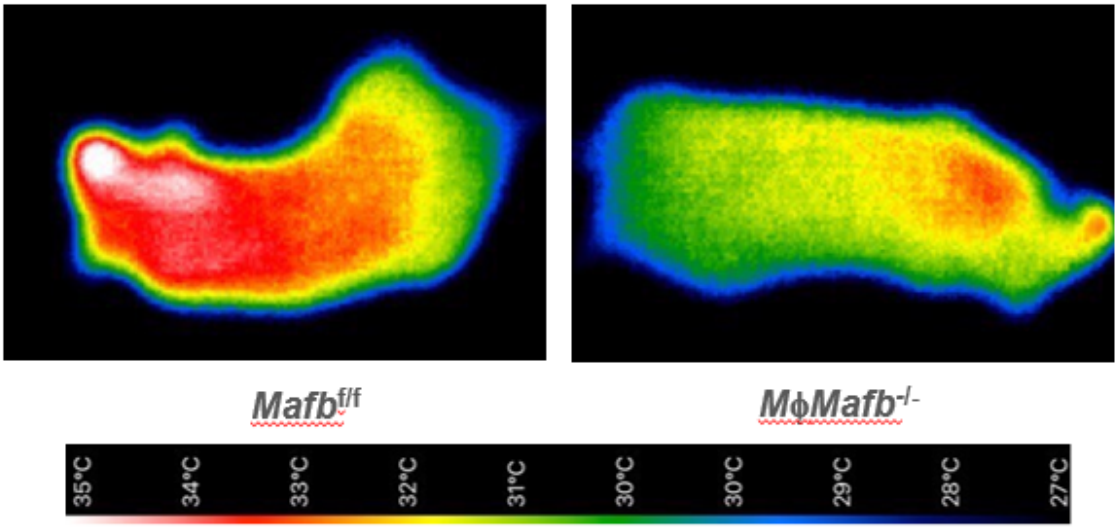

F

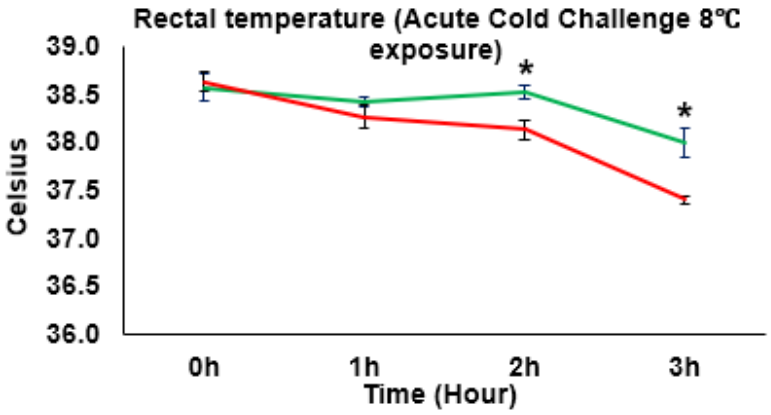

G

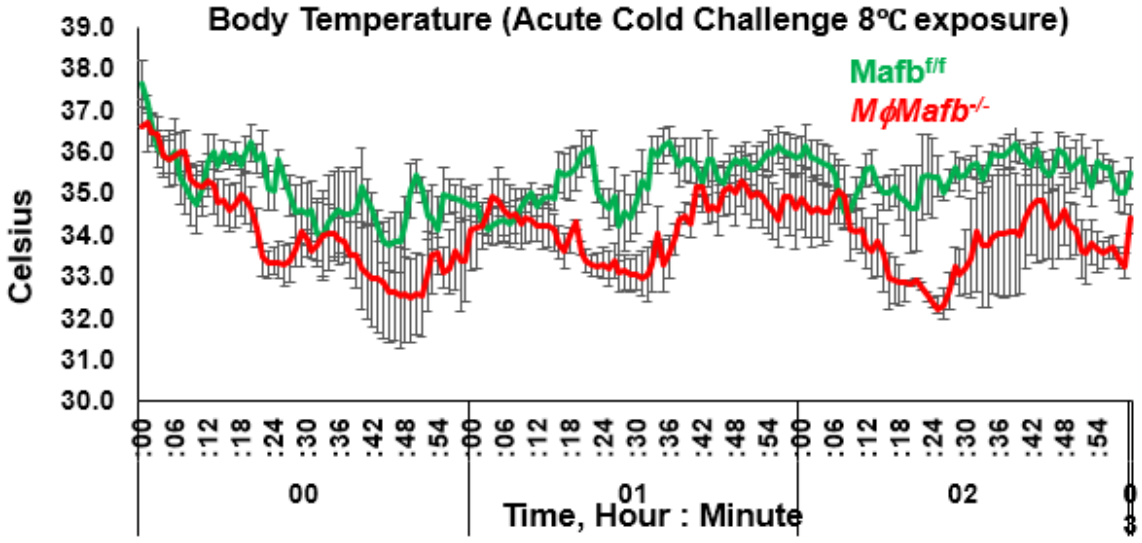

Figure 2 (H-J)

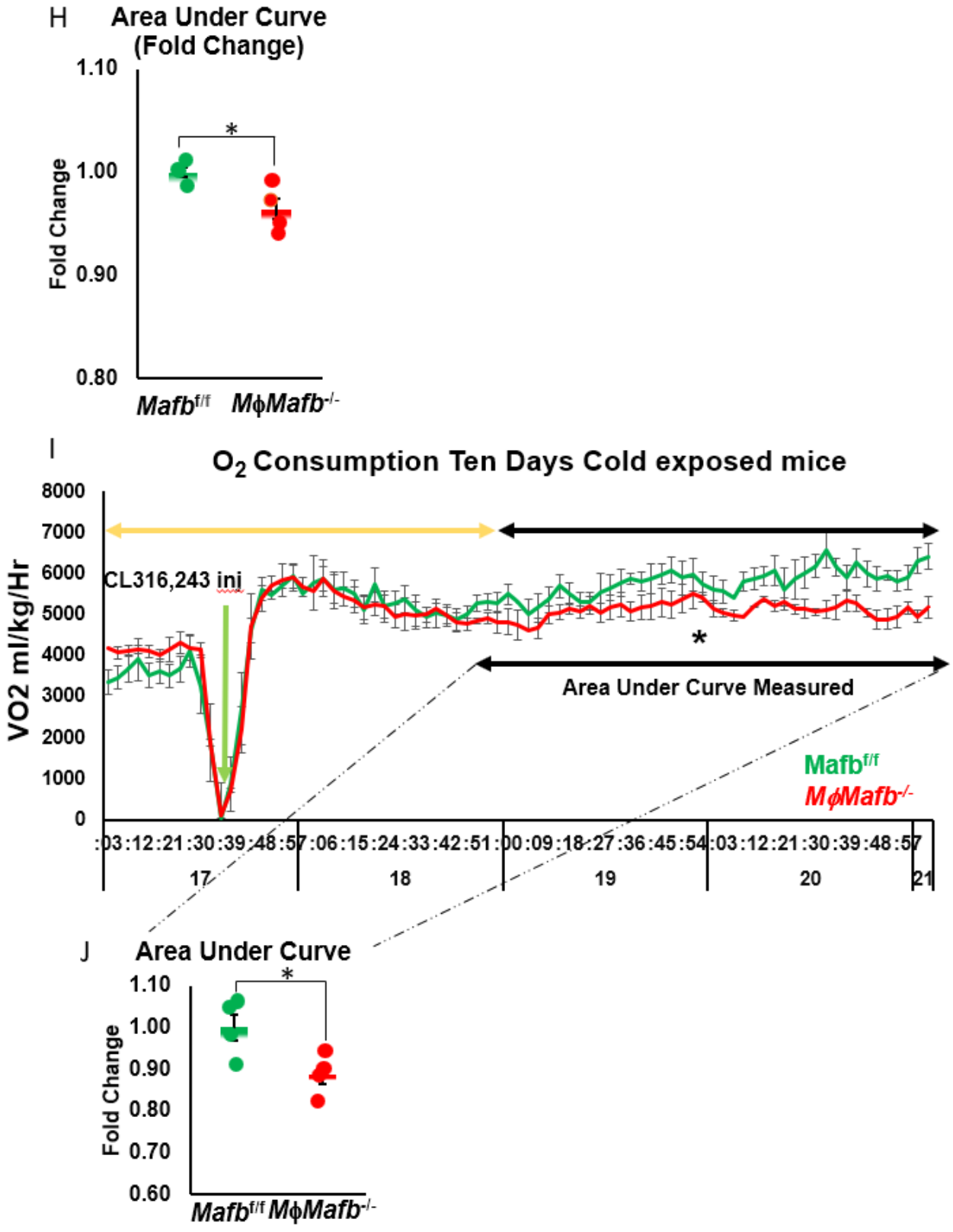
H
Area Under Curve
(Fold Change)
1.10
1.00
0.90
0.80
Fold Change
*
Mafb f/f
MϕMafb -/-
I
O2 Consumption Ten Days Cold exposed mice
8000
7000
6000
5000
4000
3000
2000
1000
0
VO2 ml/kg/Hr
CL316,243 ini
*
Area Under Curve Measured
Mafb f/f
MϕMafb -/-
:03:12:21:30:39:48:57:06:15:24:33:42:51:00:09:18:27:36:45:54:03:12:21:30:39:48:57
17
18
19
20
21
J
Area Under Curve
1.10
1.00
0.90
0.80
0.70
0.60
Fold Change
*
Mafb f/f
MϕMafb -/-

Figure 3 (A-D)

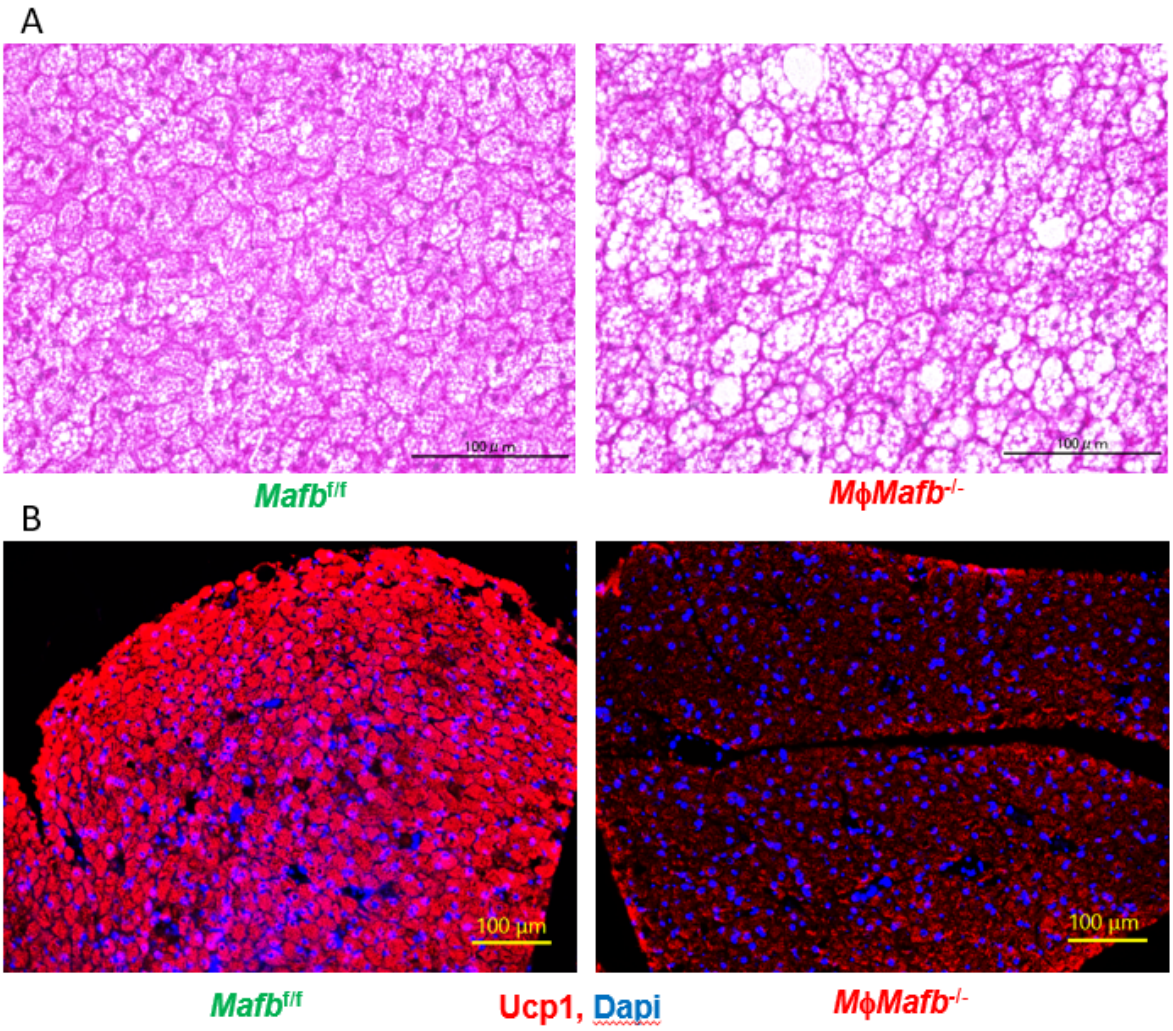
A
100 µm
100 µm
Mafb f/f
MϕMafb -/-
B
100 µm
100 µm
Mafb f/f
Ucp1, Dapi
MϕMafb -/-

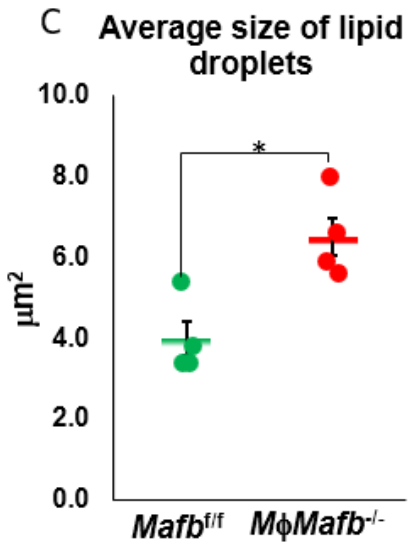
C
Average size of lipid droplets
10.0
8.0
6.0
4.0
2.0
0.0
µm2
*
Mafb f/f
MϕMafb -/-

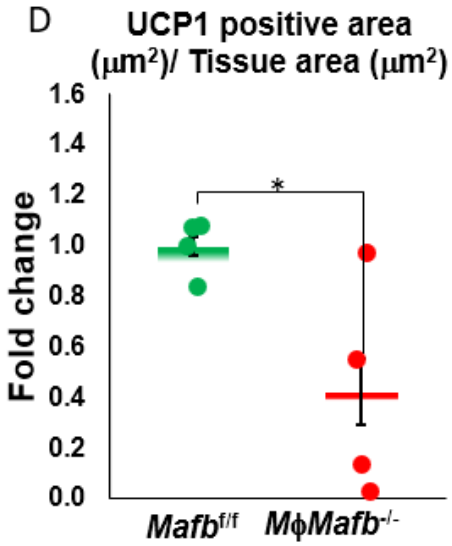
D
UCP1 positive area (µm2)/ Tissue area (µm2)
1.6
1.4
1.2
1.0
0.8
0.6
0.4
0.2
0.0
Fold change
*
Mafb f/f
MϕMafb -/-

Figure 3 (E-I)

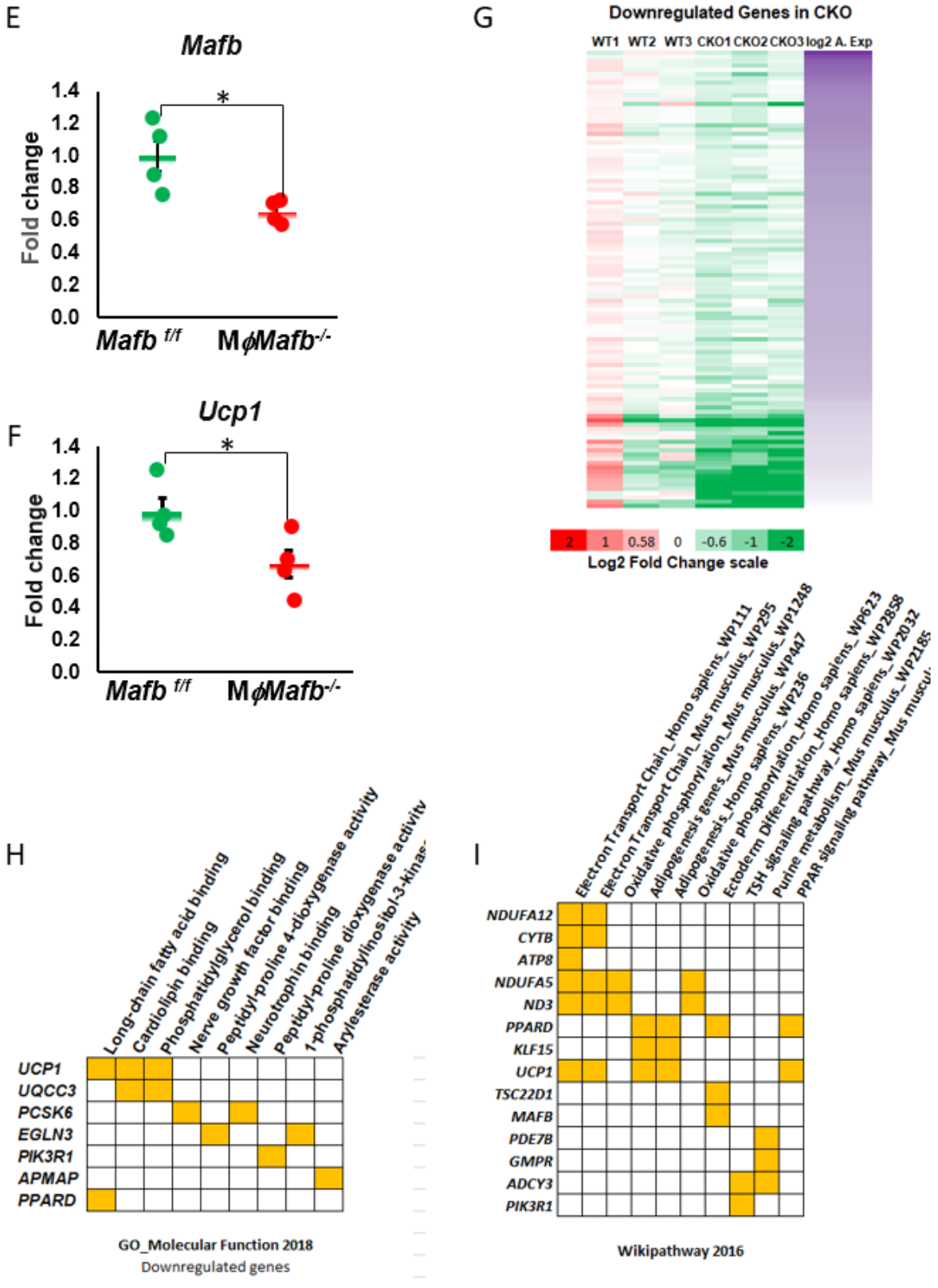
E
Mafb
Fold change
1.4
1.2
1.0
0.8
0.6
0.4
0.2
0.0
*
Mafb f/f
MϕMafb-/-
F
Ucp1
Fold change
1.4
1.2
1.0
0.8
0.6
0.4
0.2
0.0
*
Mafb f/f
MϕMafb-/-
G
Downregulated Genes in CKO
WT1 WT2 WT3 CKO1 CKO2 CKO3 log2 A. Exp
2 1 0.58 0 -0.6 -1 -2
Log2 Fold Change scale
H
Long-chain fatty acid binding
Cardiolipin binding
Phosphatidylglycerol binding
Nerve growth factor binding
Peptidyl-proline 4-dioxygenase activity
Neurotrophin binding
Peptidyl-proline dioxygenase activity
1-phosphatidylinositol-3-kinas
Arylesterase activity
UCP1
UQCC3
PCSK6
EGLN3
PIK3R1
APMAP
PPARD
GO_Molecular Function 2018
Downregulated genes
I
Electron Transport Chain_Homo sapiens_WP111
Electron Transport Chain_Mus musculus_WP295
Oxidative phosphorylation_Mus musculus_WP1248
Adipogenesis genes_Mus musculus_WP447
Adipogenesis_Homo sapiens_WP236
Oxidative phosphorylation_Homo sapiens_WP623
Ectoderm Differentiation_Homo sapiens_WP2858
TSH signaling pathway_Homo sapiens_WP2032
Purine metabolism_Mus musculus_WP2185
PPAR signaling pathway_Mus musculus
NDUFA12
CYTB
ATP8
NDUFA5
ND3
PPARD
KLF15
UCP1
TSC22D1
MAFB
PDE7B
GMPR
ADCY3
PIK3R1
Wikipathway 2016

Figure 3 (J)

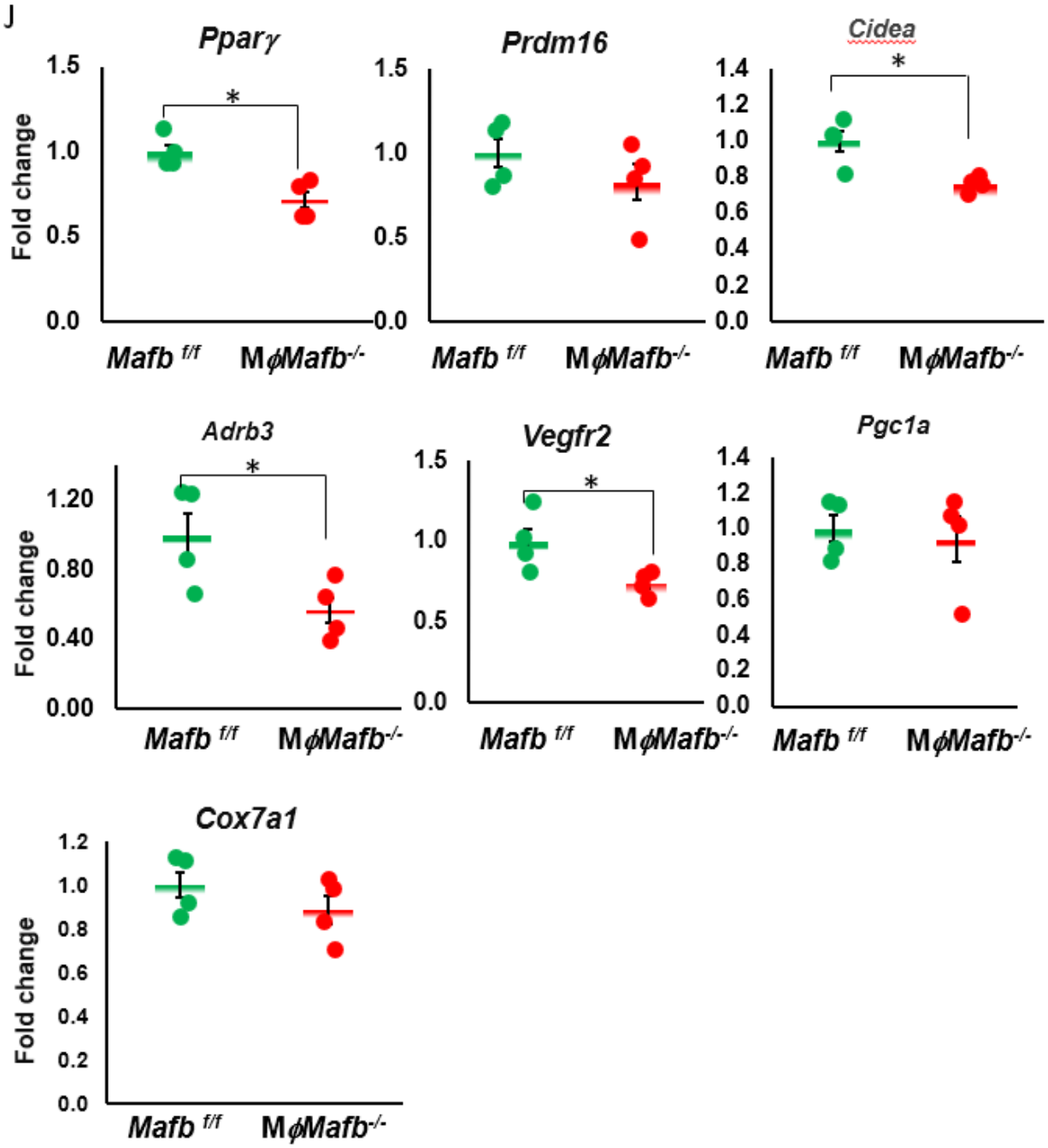
J
Pparγ
Prdm16
Cidea
Adrb3
Vegfr2
Pgc1a
Cox7a1
Fold change
Mafb f/f
MϕMafb-/-
*

Figure 4 (A-C)

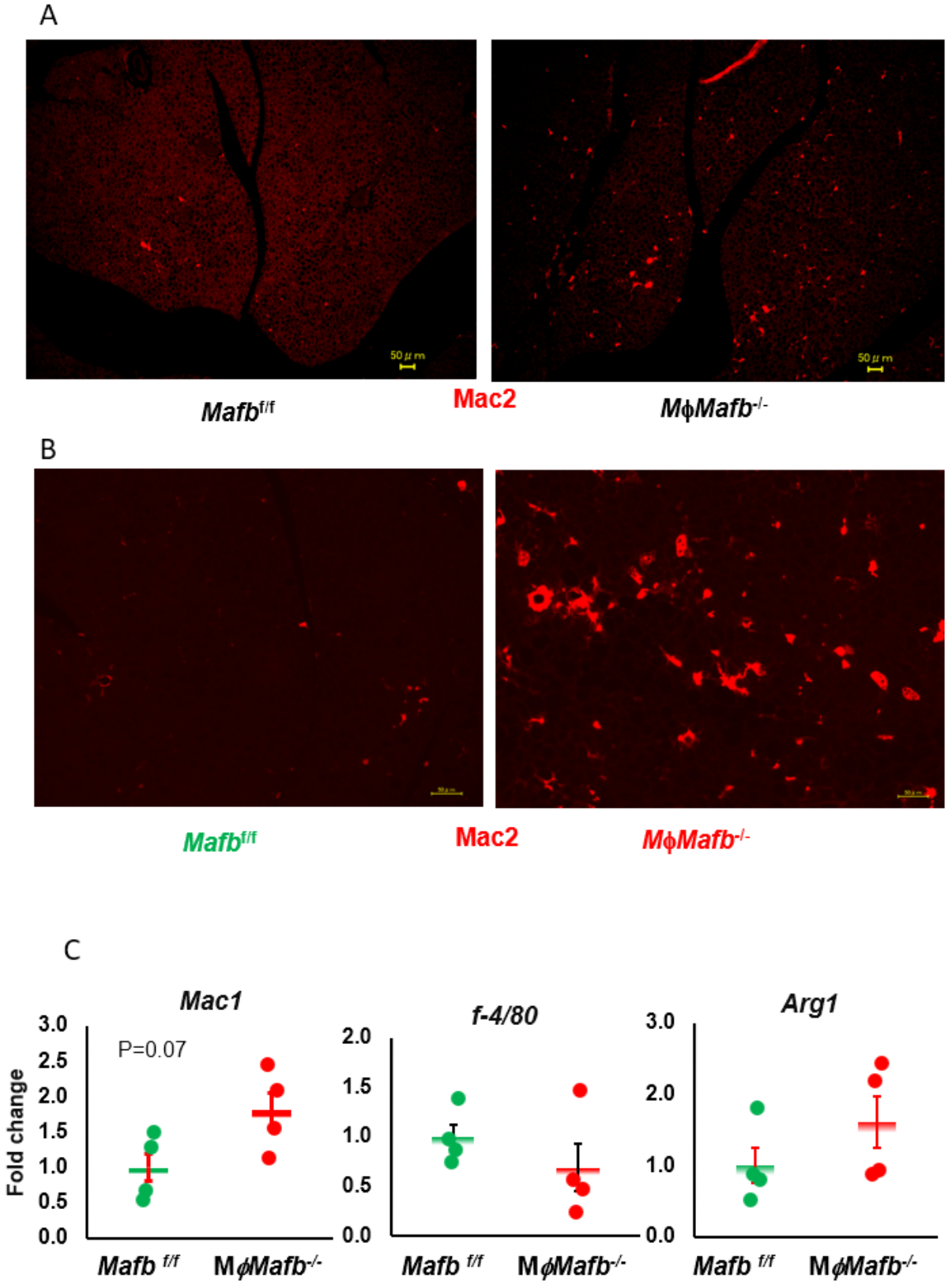
A
50 μm
50 μm
Mafb f/f
Mac2
MϕMafb -/-
B
Mafb f/f
Mac2
MϕMafb -/-
C
Mac1
P=0.07
Fold change
3.0
2.5
2.0
1.5
1.0
0.5
0.0
Mafb f/f
MϕMafb -/-
f-4/80
2.0
1.5
1.0
0.5
0.0
Mafb f/f
MϕMafb -/-
Arg1
3.0
2.0
1.0
0.0
Mafb f/f
MϕMafb -/-

Figure 4 (D-F)

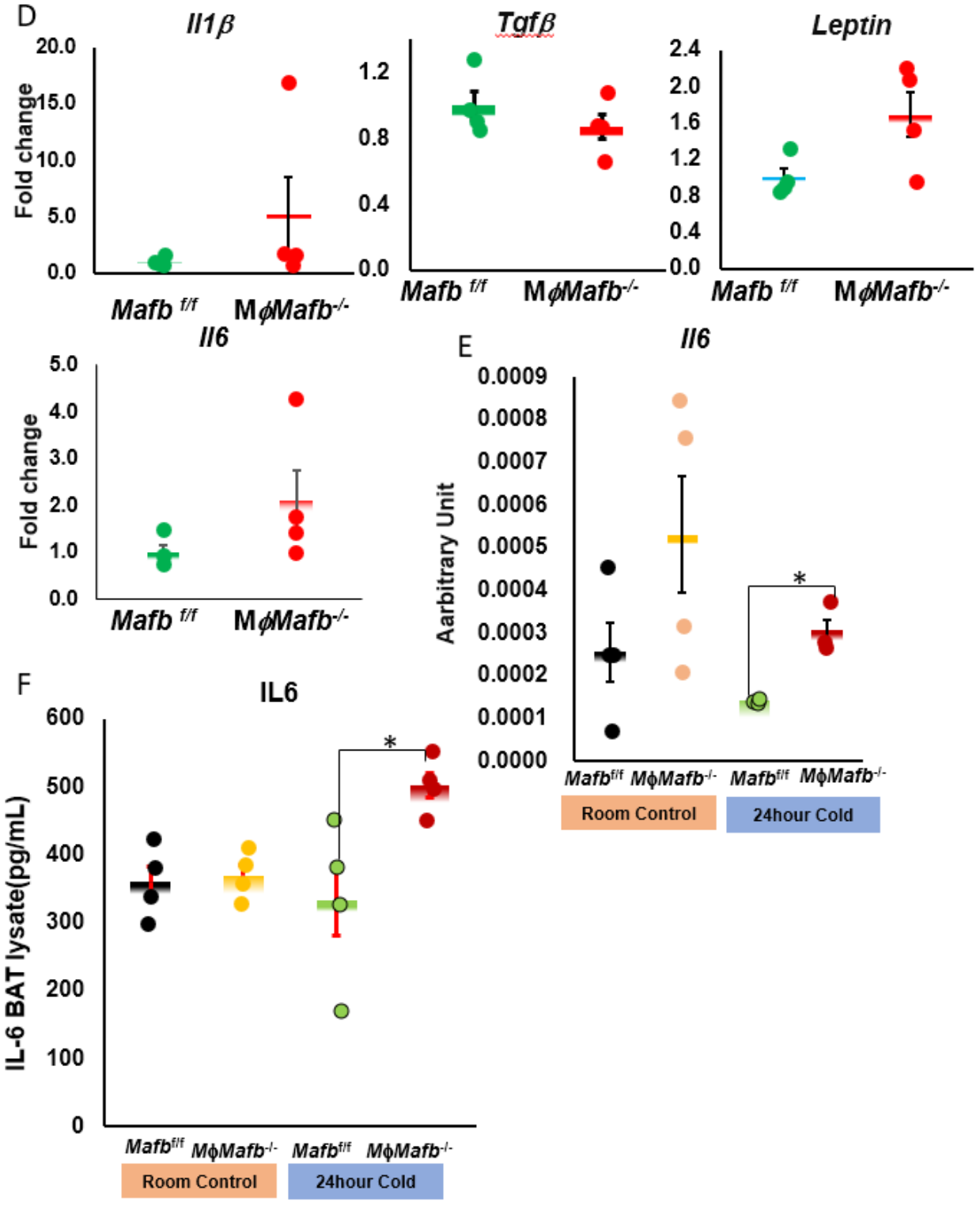
D
Il1β
Fold change
20.0
15.0
10.0
5.0
0.0
Mafb f/f
MϕMafb-/-
Tgfβ
1.2
0.8
0.4
0.0
Leptin
2.4
2.0
1.6
1.2
0.8
0.4
0.0
Il6
5.0
4.0
3.0
2.0
1.0
0.0
E
Il6
Aarbitrary Unit
0.0009
0.0008
0.0007
0.0006
0.0005
0.0004
0.0003
0.0002
0.0001
0.0000
*
Mafbf/f MϕMafb-/- Mafbf/f MϕMafb-/-
Room Control
24hour Cold
F
IL6
IL-6 BAT lysate(pg/mL)
600
500
400
300
200
100
0
*
Mafbf/f MϕMafb-/- Mafbf/f MϕMafb-/-
Room Control
24hour Cold

Figure 4 (G-I)

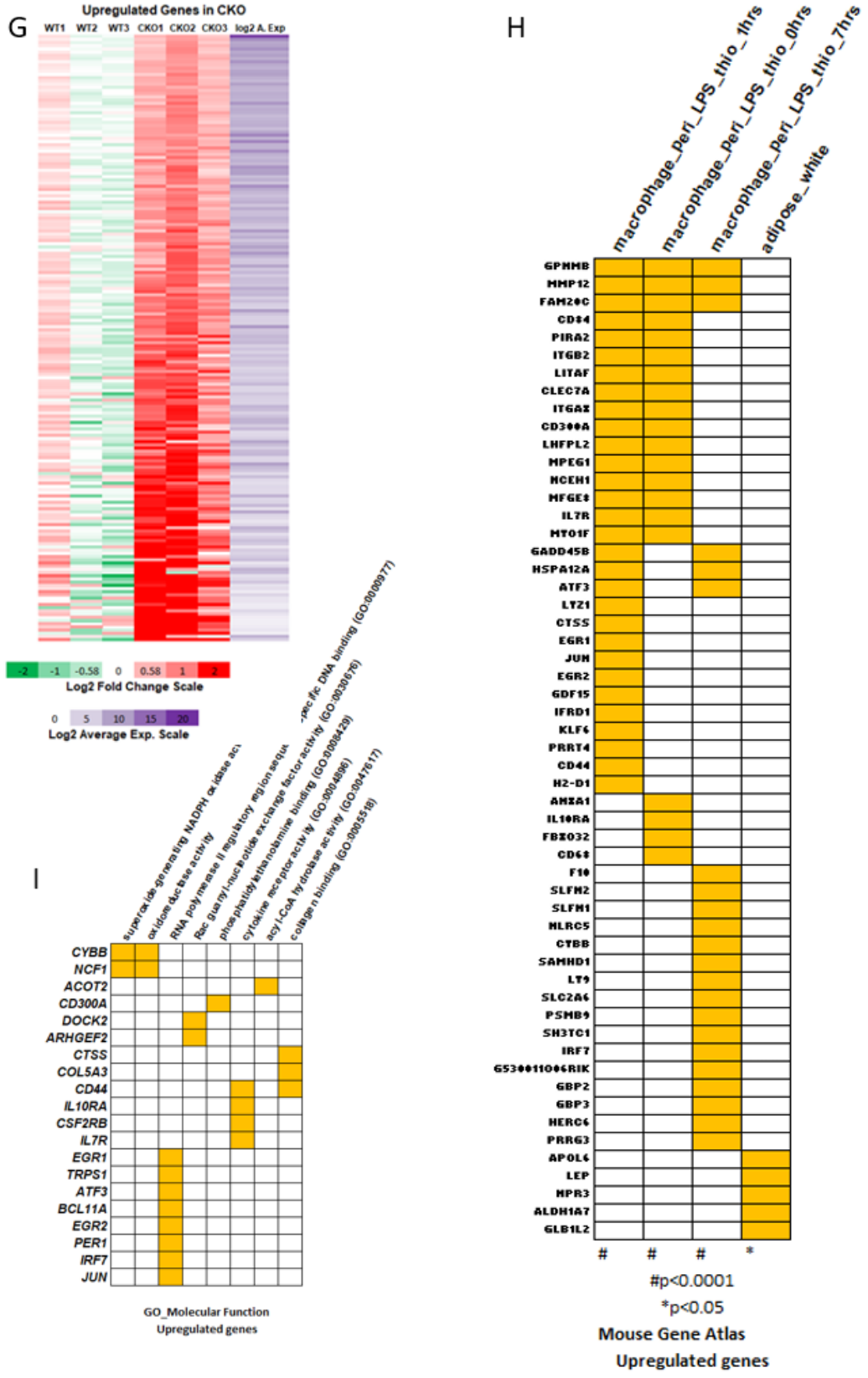
G
Upregulated Genes in CKO
WT1 WT2 WT3 CKO1 CKO2 CKO3 log2 A. Exp
-2 -1 -0.58 0 0.58 1 2
Log2 Fold Change Scale
0 5 10 15 20
Log2 Average Exp. Scale
H
macrophage_Peri_LPS_thio_1hrs
macrophage_Peri_LPS_thio_0hrs
macrophage_Peri_LPS_thio_7hrs
adipose_white
GPNMB
MMP12
FAM20C
CD84
PIRA2
ITGB2
LITAF
CLEC7A
ITGAX
CD300A
LHFPL2
MPEG1
NCEH1
MFGE8
IL7R
MT01F
GADD45B
HSPA12A
ATF3
LTZ1
CTSS
EGR1
JUN
EGR2
GDF15
IFRD1
KLF6
PRRT4
CD44
H2-D1
AMZA1
IL10RA
FBXO32
CD68
F10
SLFN2
SLFN1
NLRC5
CTBB
SAMHD1
LY9
SLC2A6
PSMB9
SH3TC1
IRF7
G530011006RIK
GBP2
GBP3
HERC6
PRRG3
APOL6
LEP
MPR3
ALDH1A7
GLB1L2
*
#p<0.0001
*p<0.05
Mouse Gene Atlas
Upregulated genes
I
superoxide generating NADPH oxidase act
oxidoreductase activity
RNA polymerase II regulatory region sequ
Rac guanyl-nucleotide exchange factor activity (GO:0005089)
phosphatidylethanolamine binding (GO:0008429)
cytokine receptor activity (GO:0004896)
acyl-CoA hydrolase activity (GO:0047617)
collagen binding (GO:0005518)
CYBB
NCF1
ACOT2
CD300A
DOCK2
ARHGEF2
CTSS
COL5A3
CD44
IL10RA
CSF2RB
IL7R
EGR1
TRPS1
ATF3
BCL11A
EGR2
PER1
IRF7
JUN
GO_Molecular Function
Upregulated genes

Figure 5 (A-B)

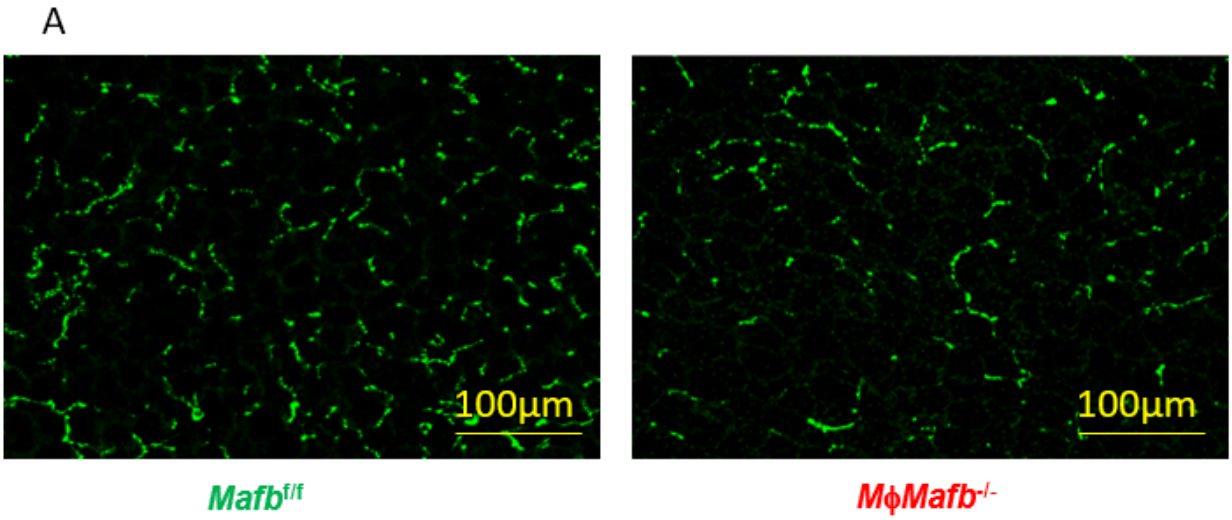
A
100µm
100µm
Mafb^f/f
MϕMafb^-/-

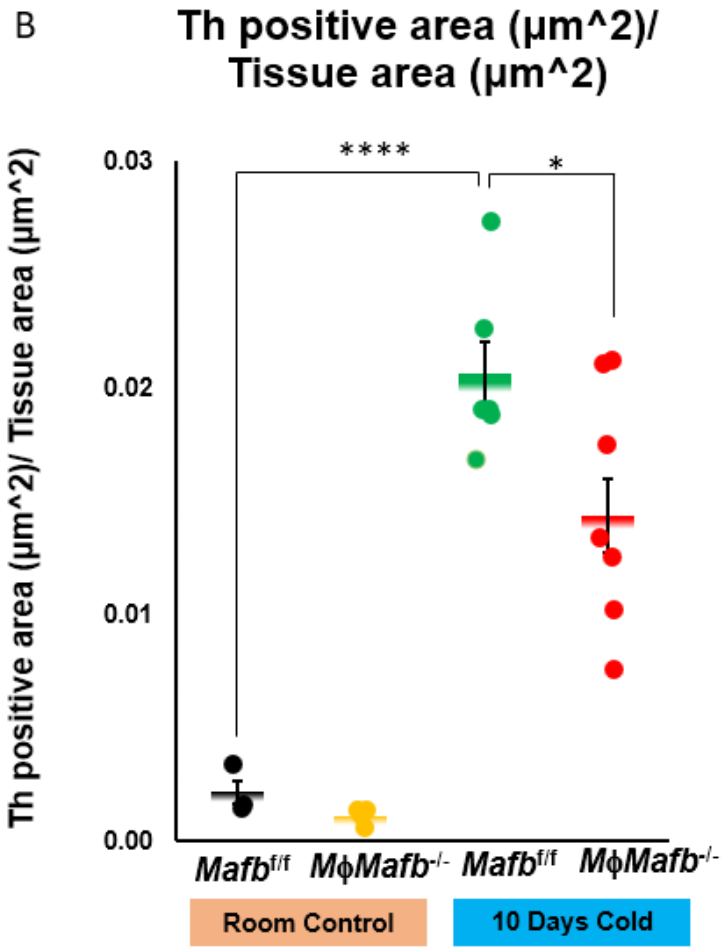
B
Th positive area (µm^2)/
Tissue area (µm^2)
Th positive area (µm^2)/ Tissue area (µm^2)
0.03
0.02
0.01
0.00
****
*
Mafb^f/f
MϕMafb^-/-
Mafb^f/f
MϕMafb^-/-
Room Control
10 Days Cold

Figure 5 (C-E)

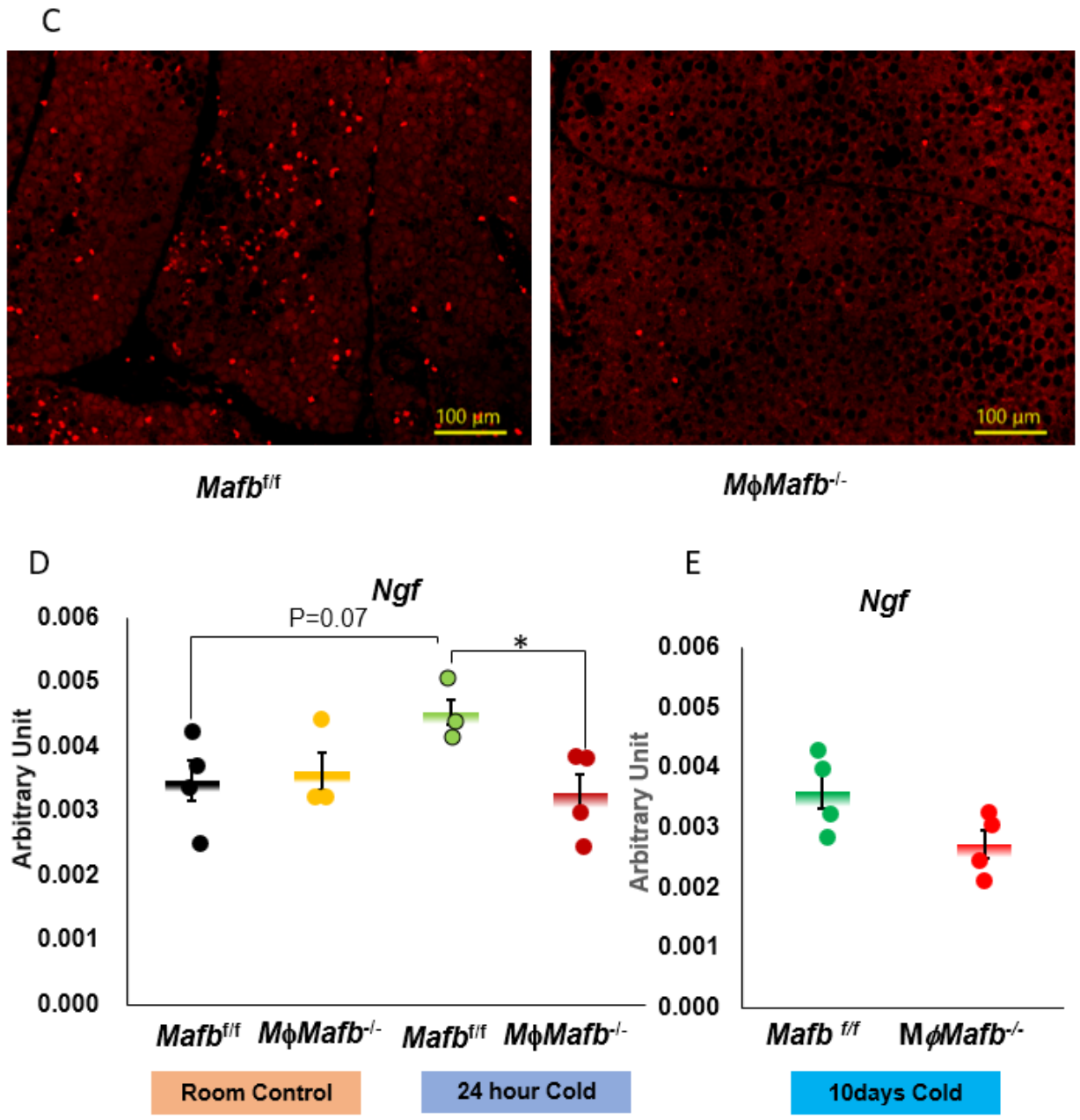
C
100 µm
100 µm
Mafb f/f
MϕMafb -/-
D
Ngf
P=0.07
*
Arbitrary Unit
0.006
0.005
0.004
0.003
0.002
0.001
0.000
Mafb f/f
MϕMafb -/-
Mafb f/f
MϕMafb -/-
Room Control
24 hour Cold
E
Ngf
Arbitrary Unit
0.006
0.005
0.004
0.003
0.002
0.001
0.000
Mafb f/f
MϕMafb -/-
10days Cold

Figure 6 (A-C)

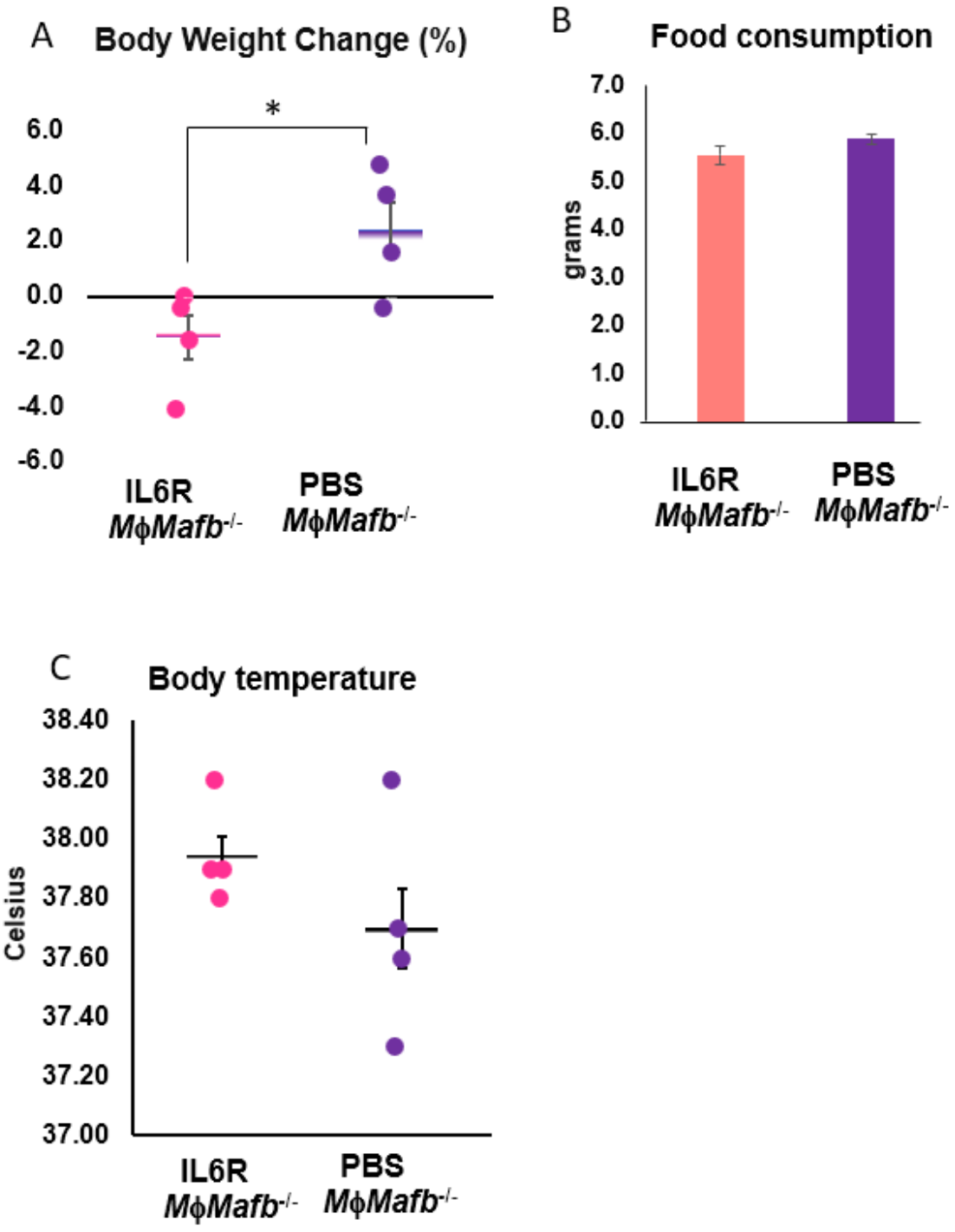
A
Body Weight Change (%)
*
6.0
4.0
2.0
0.0
-2.0
-4.0
-6.0
IL6R MϕMafb-/-
PBS MϕMafb-/-
B
Food consumption
grams
7.0
6.0
5.0
4.0
3.0
2.0
1.0
0.0
IL6R MϕMafb-/-
PBS MϕMafb-/-
C
Body temperature
Celsius
38.40
38.20
38.00
37.80
37.60
37.40
37.20
37.00
IL6R MϕMafb-/-
PBS MϕMafb-/-

Figure 6 (D)

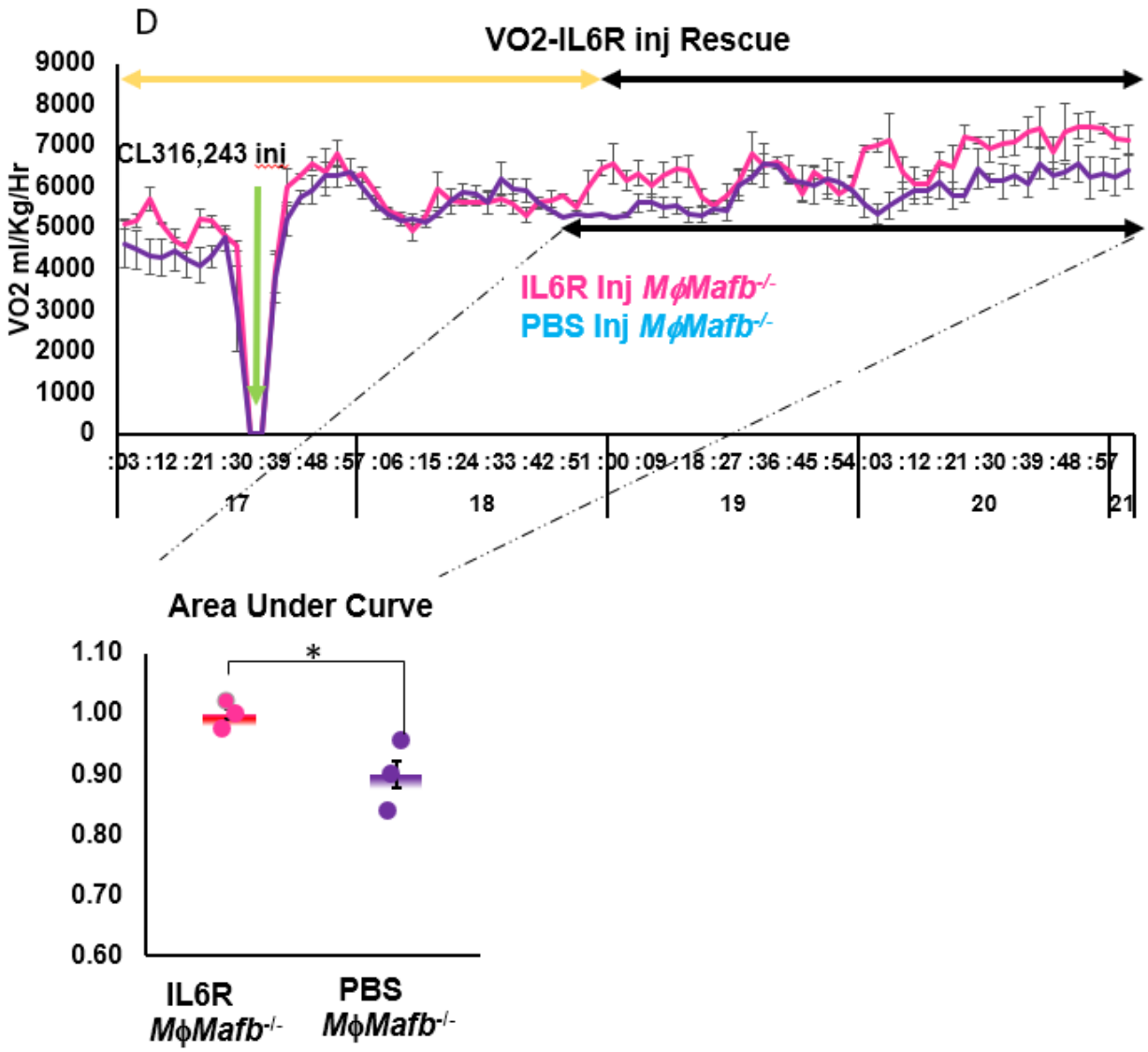
D
VO2-IL6R inj Rescue
VO2 ml/Kg/Hr
9000
8000
7000
6000
5000
4000
3000
2000
1000
0
CL316,243 ini
IL6R Inj MϕMafb-/-
PBS Inj MϕMafb-/-
:03 :12 :21 :30 :39 :48 :57 :06 :15 :24 :33 :42 :51 :00 :09 :18 :27 :36 :45 :54 :03 :12 :21 :30 :39 :48 :57
17
18
19
20
21
Area Under Curve
1.10
1.00
0.90
0.80
0.70
0.60
*
IL6R MϕMafb-/-
PBS MϕMafb-/-

Figure 7 (Summary)

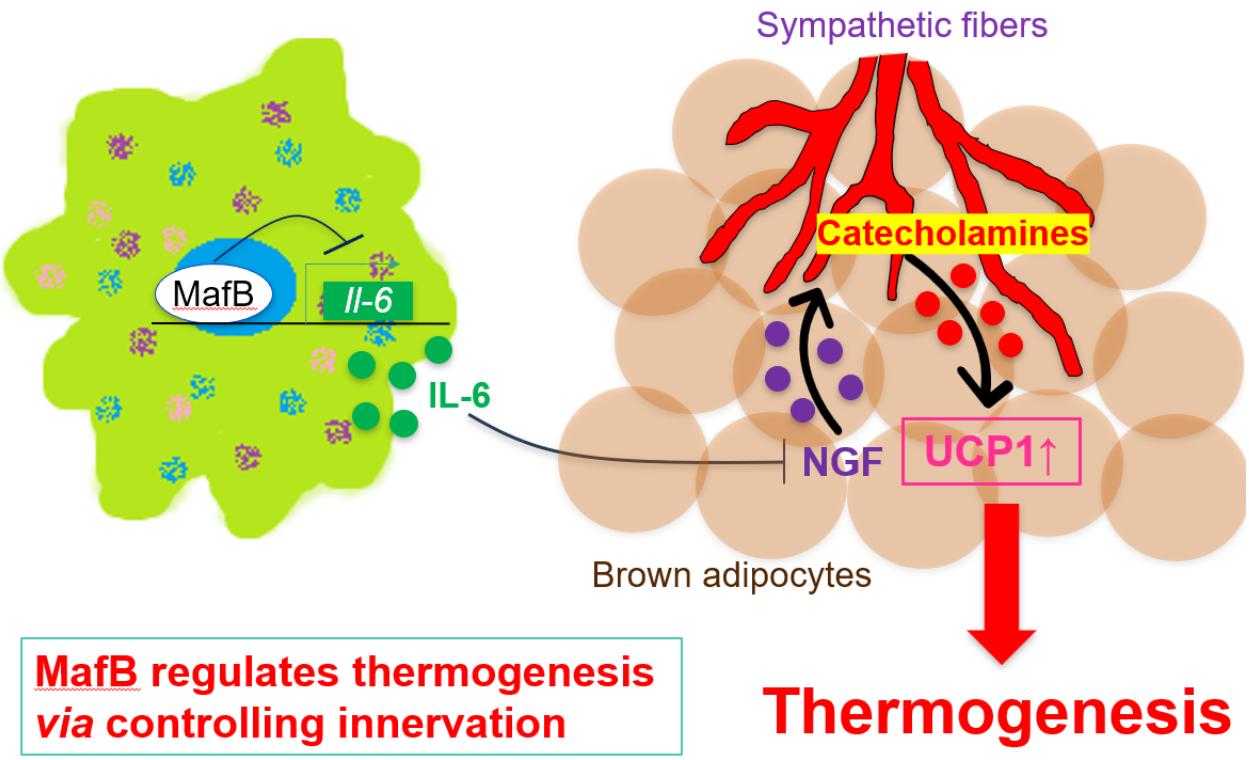

Acknowledgement

I am pleased to express my gratitude to my supervisor Prof. Satoru Takahashi for his constant help, support, encouragement, and providing me with the best platform in his laboratory where I have achieved my initial scientific carrier goals full of enjoyment. I am profoundly grateful and pay special gratitude to Dr. Michito Hamada for his continuous discussions to shape up this work. I could be able to perform only because of his excellent guidance and encouragement at every point of this work.

I gratefully acknowledge the contributions made by Ms. Megumi Ishida in this work and performing many of the experiments with me. I would like to thank all of the current and formers Dr. Hamada's group members in the Takahashi laboratory and their endless support for assisting my experiments with their experiences. I am incredibly grateful to all people in Dr. Hamada's group, who did common use of mouse colony management used in this work as well as their work as a team. I am also thankful to Ms. Olivia for her contributions as an exchange student on joining my project and performing some of the experiments.

I am very thankful to Dr. Akihiro Kuno for helping and teaching me for the RNA sequencing data analysis. I want to thank all the current and former members of the Takahashi Laboratory for their support and for working as a team. I am especially very thankful to Ms. Masami Ojima for her technical assistance all the time. I also pay special gratitude to Ms. Yukiyo Ida for her caring and providing help for purchasing materials required during the experiment. Moreover, I am delighted to thank all senior Ph.D. students of me in the Takahashi laboratory and were good friends also that includes; Dr. Kaushalya Kulathunga, Dr. Megumi Kato, Dr. Yunshin Jung, and Dr. Yuki Tsunakawa.

I am very thankful and pay special gratitude to my Ph.D. dissertation committee members Prof. Hitoshi Shimano, Prof. Taka-Aki Sato, Prof. Kazuko Shibuya, and Prof. Seong-Jin Kim for their constructive guidance and time.

I also pay particular gratitude to Prof. Masato Tanaka and his Laboratory "Laboratory of Immune Regulation, Tokyo University of Pharmacy and Life Science" for teaching me special techniques of macrophages study. I am also thankful to Dr. Gen Nishitai and Dr. Kenichi Asano for their kind assistance during the lab rotation in Tanaka Laboratory.

I am incredibly grateful to all faculty of the Human Biology Program and SIGMA staff for their kind support. I gratefully acknowledge the financial support by the "Japan Society for the Promotion of Science" (JSPS) and Japan's "Ministry of Education, Culture, Sports, Science & Technology" (MEXT).

Finally, I would like to thank my Family, Friends, and Relatives who supported me throughout my life. I am especially very thankful to some of my friends and seniors who helped me a lot that includes Mr. Manoj Kumar (Jamia Hamdard, New Delhi), Mr. Lalhabba Oinam, Mr. Lokesh Agrwal, Mr. Yaqiu Wang, Mr. Rupesh Choudhary, Dr. Rahul Sharma, Mr. Manoj Kumar (Prabhakar), Mr. Ritesh Patel, Mr. Deepak Kumar, Mr. Navneet Pandey, and Ms. Rekha Dubey.